PROCEEDINGS OF THE 24TH INTERNATIONAL APPLIED GEOCHEMISTRY SYMPOSIUM

FREDERICTON, NEW BRUNSWICK, CANADA

JUNE 1ST-4TH, 2009

EDITED BY

DAVID R. LENTZ, KATHLEEN G. THORNE, & KRISTY-LEE BEAL

VOLUME II

All rights reserved.
This publication may not be reproduced in whole or in part, stored in a retrieval system or transmitted in any form or by any means without permission from the publisher.

ISBN 978-1-55131-137-1 (Volume 2)

©2009 AAG

PROCEEDINGS OF THE 24TH INTERNATIONAL APPLIED GEOCHEMISTRY SYMPOSIUM

FREDERICTON, NEW BRUNSWICK
CANADA
JUNE 1ST-4TH, 2009

EDITED BY

DAVID R. LENTZ
KATHLEEN G. THORNE
KRISTY-LEE BEAL

VOLUME II

TECHNICAL EDITORS

(Listed in alphabetical order)

Mark Arundell
U. Aswathanarayana
Roger Beckie
Chris Benn
Robert Bowell
Charles Butt
Bill Coker
Hugh deSouza
Sara Fortner
David Gladwell
Wayne Goodfellow
Eric Grunsky
William Gunter
Gwendy Hall
Jacob Hanley
Russell Harmon
David Heberlein
Brian Hitchon
Andrew Kerr
Dan Kontak
Kurt Kyser
David Lentz
Ray Lett
Matthew Leybourne
Steven McCutcheon
Beth McClenaghan
Nancy McMillan
Paul Morris
Lee Ann Munk
Dogan Paktunc
Roger Paulen
Ernie Perkins
David Quirt
Andy Rencz
David Smith
Cliff Stanley
Gerry Stanley
Nick Susak
Bruce Taylor
Ed Van Hees
James Walker
Lawrence Winter

GENERAL SESSION

EDITED BY:

DAVID R. LENTZ

Investigation of physical, chemical and microbiological processes in the development of forest rings in Ontario

Kerstin Brauneder [1], Stewart M. Hamilton[2], Keiko H. Hattori[1], & Gordon Southam[3]

[1]*University of Ottawa, 140 Louis Pasteur, Ottawa, ON, K1N 6N5 CANADA (e-mail: kbrau049@uottawa.ca)*
[2]*Ontario Geological Survey, 933 Ramsey Lake Road, Sudbury, ON P3E 2G9 CANADA*

[3]*University of Western Ontario, 1151 Richmond St.,London, ON N6A 5B7 CANADA*

ABSTRACT: Forest rings are large circular features distinctive of Ontario's boreal forest. They are centred on areas of negative redox charge and characterized by a slight depression in the mineral soil around the edge of the ring. A field and laboratory investigation of forest rings is examining the complex relationship between physical, chemical and microbiological processes occurring at the edge of these features. Physical changes that are known to occur include a slight positive electrical field anomaly over the centre of the ring, a negative thermal and hydraulic-conductivity anomaly. Chemical changes are profound and most exemplified by a very sharp redox gradient at the edge of the ring between the chemically reduced interior and the oxidized exterior. Microbiological processes are also occurring and although cause-and-effect relationships are still unproven, they may be crucial in the formation of the rings. A four week laboratory experiment involves the *in vitro* creation of the redox gradients of the two end-member types of rings: one centred on a hydrogen sulfide source and another on a methane source. Test-tubes are being inoculated with bacteria from the highest-gradient ring parts of the respective ring edges. Measurements will provide insight on the role of micro-organisms in ring formation.

KEYWORDS: *forest ring, thermal conductivity, redox, microbiology*

INTRODUCTION

Forest rings are large circular features commonly observed in the boreal forests of Ontario (Fig. 1). Over 2000 forest rings, ranging from 15 m to 1.5 km in diameter, have been identified on aerial photographs thus far. The circular impression reflects a slight topographic depression (Giroux *et al*. 2001) that forms around centres of negative charge enclosed in the overburden or bedrock. Large accumulations of shallow, biogenic methane are estimated to account for 85% of northern Ontario's forest rings (Hamilton *et al*. 2004). Forest rings have also been reported to form over accumulations of bitumen, coal and dissolved hydrogen sulfide (Hamilton & Hattori 2008). The reducing source imparts electrochemically reducing conditions in overlying and surrounding materials generating numerous physical and chemical changes at the ring edges. Most notably, subtle positive spontaneous potential (SP) anomalies can be noted in association with strong, negative-inward, redox gradients (Hamilton & Hattori 2008). The goal of our work is to understand the role of micro-organisms in the oxidation process and in the generation of electrical fields.

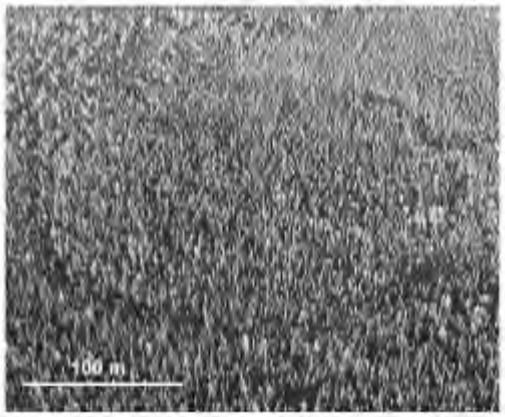

Fig. 1. Aerial view of a forest ring near Hearst, Ontario.

The current investigations monitor changes in groundwater temperature across an H_2S-centered forest ring. The rationale behind the temperature measurements was that microbiological activity and intense oxidation is known to occur at the ring edges and it was thought that temperature data might pinpoint the exact location of the associated exothermic reactions and help with energy and mass budget calculations. However, to our surprise, the results were the opposite of what had been expected; they show a significant *negative* thermal anomaly. Subsequent investigations have (1) confirmed the results, (2) shown them to occur at other rings, and (3) narrowed the location of the temperature anomaly to precisely that of the physical, chemical and microbiological changes that occur at the ring edge. The purpose of this study is to understand these changes and how they are interrelated and to investigate the role of micro-organisms in the oxidation process and generation of electrical fields at the ring edge.

METHODOLOGY

Groundwater temperatures and water levels were monitored for a period of 10 months across the edge of an H_2S-centered forest ring ("Thorn-North") located 45 km northwest of Timmins, Ontario. Measurements were made using down-hole data loggers installed in existing monitoring wells at a depth of approximately 6.5 m. In addition, the ring edges of two methane-centred forest rings ("Road ring" and "Bean") were sampled for soil and peat. High-density sampling was done at several depths on transects across the ring edges. Time-sensitive parameters such as pH and oxidation-reduction potential (ORP) were measured at the time of collection.

Clay samples were collected at areas of high-redox gradient at the edge of the Thorn-north ring and the Bean ring, which are H_2S sourced and methane sourced, respectively. These samples were preserved under anoxic conditions and are now being used for the test-tube experiments.

Clay from the ring edges was suspended in agar and served as the inoculant and the carbon source for the in-vitro growth of forest ring micro-flora. A redox gradient was established by the steady supply of oxygen at one end and a source of CH_4 or H_2S at the other end of the test tube. Changes in pH, ORP and SP were monitored over a period of four weeks.

SELECTED RESULTS

A detectable drop in groundwater temperature can be measured over the ring edge at Thorn North. Peat-waters collected during the month of July, at 1.5m depth show a minimum of 2°C within the ring edge while outside values peak at 10°C. Although the sampling site is located 200 km south of the southernmost limit of discontinuous permafrost, temperatures have remained low enough to allow the preservation of ice within the peat. The temperature anomaly is propagated to depth, with a 0.35°C anomaly occurring at the same place in groundwater from underlying clay (Fig. 2). In addition, the response of groundwater temperature to seasonal changes in air temperature is higher at the ring edge than in adjacent areas. At 6.5 m depth, the coldest month of the year is August, due to a lag in summer warming. Groundwaters in the ring edge reach their

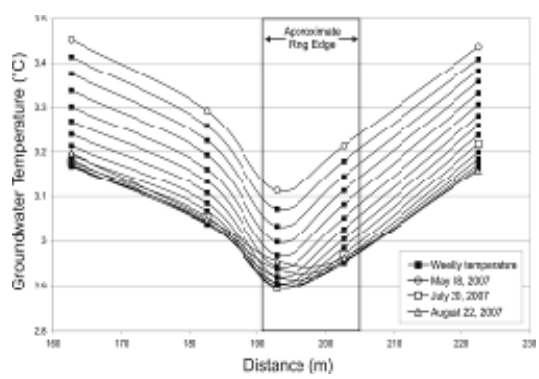

Fig. 2. Changes in mean weekly groundwater temperatures (6.5 m depth) across the

northern ring edge of Thorn-North from May to August 2007 (Brauneder *et al.* 2008).

coldest temperature on July 20, whereas groundwaters in adjacent areas reach their coldest state one month later. Similarly, data collected from November to December shows that groundwaters within the ring edge reach their warmest temperature one month earlier than in adjacent areas.

The most likely reason for the thermal anomaly at the ring edge is that it coincides with an area of increased thermal conductivity in the clays. This area also coincides with an area of decreased hydraulic conductivity (Fig. 3).

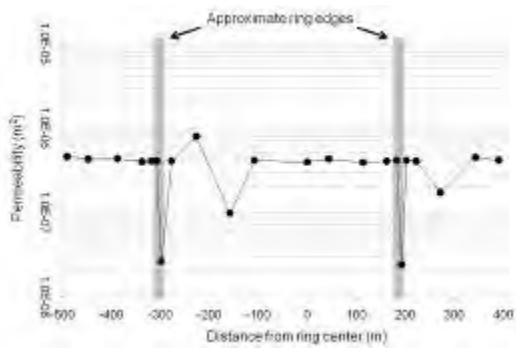

Fig. 3. Changes in permeability along a 900 m long transect crossing Thorn-North from south to north.

These physical changes are accompanied by chemical changes. Most notably, a sudden and strong redox gradient, pH gradient and oxygen depletion occur on all investigated ring edges. Similar responses have been noted at other rings. Figure 4 shows an ORP change of 200 mV occurring over a distance of only 3 m at the edge of the Road ring and known to be associated with a pH increase of 0.5 units.

MICROBIOLOGICAL INVOLVEMENT

Redox gradients as strong as those observed at the ring edges are potential sources of energy for autotrophic bacteria. Evidence for microbial involvement includes H_2S consumption, SO_4^{2-} enrichment, oxygen depletion in the

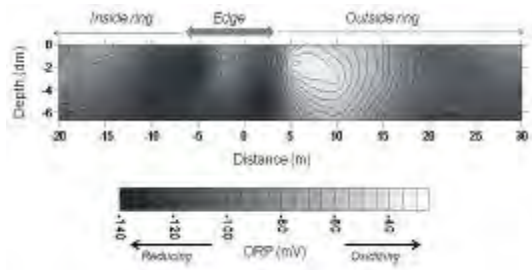

Fig. 4. ORP profiling of the top first meter of clay across the northern edge of the Road ring.

headspace of wells and minor to major biogenic methane production. Additional evidence is given by the generation of hydrocarbons at a number of rings.

The ongoing microbiological experimentation attempts to re-create *in vitro*, the redox conditions at the edge of two types of forest rings: those centred on methane and H_2S. A redox gradient is being established between each of these reducing agents and oxygen. Test-tubes will be inoculated with bacteria collected from the highest redox-gradient areas on each ring type. Measurements over the course of the 4 week experiment will help to determine the complex cause-and-effect relationships that exist between the physical, chemical and microbiological processes occurring at the ring edge.

CONCLUSIONS

A large number of physical and chemical changes occur in overburden and groundwater at the edges of forest rings. Physical changes include an apparent increase in thermal conductivity and a decrease in hydraulic conductivity. Chemical changes are dominated by a very strong and sudden change from reducing to oxidizing conditions at the ring edge. These changes are all spatially related. Broadly speaking the changes follow the model of Hamilton & Hattori (2008) but unexpected developments, including the thermal anomaly, have been uncovered. Furthermore that model does

not consider the involvement of micro-flora, which may be an important or even crucial factor in the development of forest rings.

ACKNOWLEDGEMENTS

This project is part of the first author's Master's thesis. It is supported in part through a Natural Sciences and Engineering Research Council (NSERC) grant to Keiko Hattori at the University of Ottawa, the Ontario Geological Survey, and through grants from the Society of Economic Geologists and the American Association of Petroleum Geologists.

REFERENCES

BRAUNEDER, K., HAMILTON, S.M., & HATTORI, K.H. 2008. Detailed investigation of chemical and microbiological parameters over forest-ring edges in northern Ontario. In: *Summary of Field Work and Other Activities 2008*. Ontario Geological Survey, Open File Report, **6226**, 28-1 to 28-8.

GIROUX, J.F., BERGERON, Y., & VEILLETTE, J.J. 2001. Dynamics and morphology of giant circular patterns of low tree density in black spruce stands in northern Quebec. *Canadian Journal of Botany,* **79**, 420–428.

HAMILTON, S.M., BURT, A.K., HATTORI, K.H., & SHIROTA, J. 2004. The distribution and source of forest ring-related methane in northeastern Ontario. In: *Summary of Field Work and Other Activities 2004*. Ontario Geological Survey, Open File Report, **6145**, 21-1 to 21-26.

HAMILTON, S.M. & HATTORI, K.H. 2008. Spontaneous potential and redox responses over a forest ring. *Geophysics*, **73**, B67–B75.

Geology and Geochemistry of the Lac Cinquante Uranium Deposit, Nunavut

Nathan J. Bridge[1], Neil R. Banerjee[1], Craig S. Finnigan[1,2], Rob Carpenter[2,3], & Jeff Ward[3]

[1]*Department of Earth Sciences, University of Western Ontario, London, ON, Canada, N6A5B7*
[2]*Kaminak Gold Corporation, Suite 1440 – 625 Howe St., Vancouver, BC, Canada, V6C 2T6*
[3]*Kivalliq Energy Corporation, Suite 1440 – 625 Howe St., Vancouver, BC, Canada, V6C 2T6*

ABSTRACT: The Lac Cinquante uranium deposit is located in the Hearne Subprovince of the Western Churchill Province, in the Kivalliq region of Nunavut. Lac Cinquante is hosted in a basement of Archean greenstones that are unconformably overlain by Proterozoic sediments. In this study we present a newly acquired detailed geological map of the Lac Cinquante region that has been coupled with bulk rock geochemistry in an attempt to understand the formation of the Lac Cinquante uranium deposit. This new geological and geochemical information reveal a more detailed geological history than previously reported. Preliminary oxygen stable isotope compositions for the rocks surrounding the main ore zone show an envelope of high $\delta^{18}O$ values, possibly related to increased low-temperature water-rock interaction, and compositional changes. Future studies at the Lac Cinquante deposit involving fluid-rock reaction and ore zone formation will be useful in unravelling the metallogenic history for the Lac Cinquante deposit and mineralization in the surrounding region.

KEYWORDS: *Unconformity Hosted Uranium Deposit, Nunavut, Geochemistry, Uranium Exploration, Oxygen Stable Isotopes*

INTRODUCTION

The Lac Cinquante unconformity associated uranium deposit is located in the Kivalliq district of Nunavut approximately 350 km west of Rankin Inlet, and is centered on approximately Latitude 62° 34'33" N, Longitude 98°41'41"W. The deposit is hosted in volcanic Archean greenstones that are unconformably overlain by the northeast trending Angikuni sub-basin. Mineralization is found within the basement volcanics that have undergone hydrothermal alteration along fault zones (Miller et al., 1986). Two major zones of mineralization, and three major styles of mineralization within the Archean greenstones have been identified in previous studies (Miller et al., 1986). Additionally, zones of anomalous uranium concentration have been recognised in the overlying Proterozoic sediments. In this study we present a detailed 1:5000 geological map that has been combined with new stable isotope and bulk rock geochemical data. Mapping and bulk-rock geochemistry have revealed a suite of Archean tholeiitic basalts and basaltic andesites that transition into a tholeiitic bimodal volcanics to the East. The entire package is unconformably overlain by Proterozoic sediments grading upwards from basal breccia, into conglomerate, and sandstone with a volcanic trachyte unit capping the sedimentary rocks. Oxygen stable isotope geochemistry reveals a zone interpreted to represent high-fluid flow and water-rock interaction associated with the mineralized metasedimentary layer in the Archean volcanics, which is important for understanding the composition, temperature, and amount of fluid responsible for the formation of the uranium deposit.

REGIONAL GEOLOGY

The Lac Cinquante uranium deposit is located in the Kivalliq Region of the Hearne Subprovince in the Western Churchill Province, Nunavut. The Western

Churchill Province is located in between the Superior province and Slave provinces and is separated from them by the Trans-Hudson and Thelon orogens (Hoffman, 1988). The Western Churchill Province has been subdivided into the Rae and Hearne subprovinces, which are seperated by the Snowbird Tectonic Zone (Hoffman, 1988; Berman et al, 2007). The deposit is associated with an Archean greenstone sliver related to the Yathkyed Greenstone belt and is unconformably overlain by the Angikuni sub-basin, one of several northeast trending Proterozoic sub-basins of the Dubawnt Supergroup (Rainbird et al., 2003).

LOCAL GEOLOGY

The Lac Cinquante region is characterized by an Archean-Proterozoic unconformity (Figure 1). The area was first mapped by Miller et al. (1986) and was re-mapped in the summer of 2008. Mapping has revealed a basement assemblage of Archean greenstonesconsisting of a package of tholeiitic meta-basites including gabbros, massive basalts, and pillowed basalts, with interlayered metasedimentary tuffs. This package appears to repeat in a cyclical manner, with gabbros at the base, grading into massive flows with pillowed tops. To the East, the Archean sequence grades into a suite of bimodal volcanics that are comprised of alternating mafic (basaltic-andesite) flows and felsic pyroclastic units. Proterozoic sediments of the Dubawnt Supergroup Baker Sequence, are located above the unconformity in the Lac Cinquante region. This sequence is characterized by a basal breccia unit at the base, overlain by clast-supported conglomerates with interbedded sandstones that fine upwards into sandstones, and siltstones. Conformably overtop of the Proterozoic sediments lies the Christopher Island Formation

MINERALIZATION

Two major zones of mineralization, the Main zone and the South Zone have been

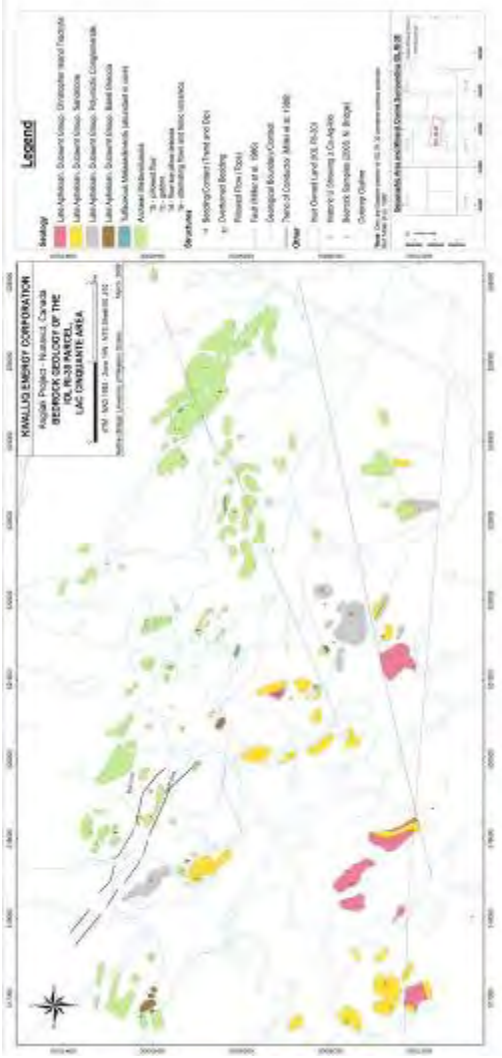

Fig.1. Geology of the Lac Cinquante region shows Archean (green rocks) and ProterozOc rocks (yellow, grey, brown, and pink) separated by an unconformity (dashed line). The location of the two major zones of mineralization, the main zone and south zone, documented by Miller et al. (1987) are noted on the map.

documented in previous studies. These are characterized by graphitic exhalative horizons, and in drill core appear as tuffaceous metasediments (Miller et al., 1986). In the region, three major styles of mineralization have been documented in the Archean greenstones, including: disseminated pitchblende with base metals in tuffaceous metasediments, discrete pitchblende veins that cut across

the metasediments, and quartz, carbonate, sulphides, and pitchblende in gash veins trending 040 to 060 along fractures (Miller et al., 1986). Future studies of the mineralization will aim to document the age of mineralization, timing of mineralization, and composition and temperature of the fluids responsible for mineralization.

BULK ROCK AND STABLE ISOTOPE GEOCHEMISTRY

Bulk rock geochemistry of the Lac Cinquante deposit shows that the Archean volcanic rocks (both the mafic volcanic flows and the bimodal volcanic suite) are dominantly tholeiitic high-Fe basalts and basaltic andesites. The alternating felsic units in the bimodal suite are dacitic and rhyolitic in composition (Fig. 2).

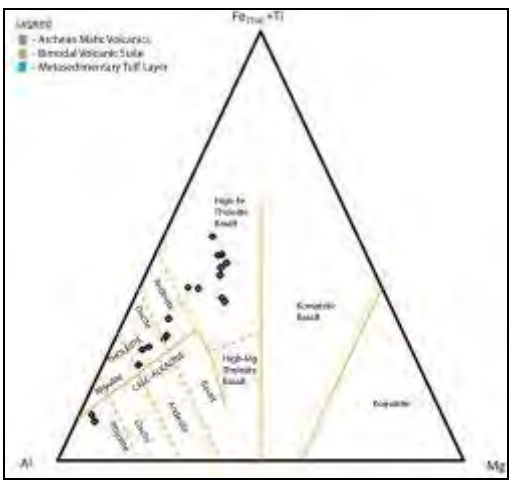

Fig. 2. Jensen cation plot for the classification of volcanic rocks in the Lac Cinquante region according to their Al, Mg, and Fe+Ti cation ratios.

Preliminary oxygen isotope data from bulk rocks in a drill core that crosses the main zone (Fig. 3) show that the rocks surrounding the main ore zone at the Lac Cinquante deposit are elevated above normal magmatic values. This has been interpreted to preserve the signature of elevated fluid flow surrounding the ore zone. The trend is characterized by a steady increase in $\delta^{18}O$ to a peak at the ore zone, and a steady decrease in $\delta^{18}O$ to more typical magmatic values after the ore zone. This may have resulted from low-temperature alteration (< 250°C) of basalt leading to the formation of secondary phyllosilicate (and other) minerals with elevated $\delta^{18}O$ values. It is also evident from this data that focused fluid flow around the deposit is likely linked to the chemistry of the rocks hosting the ore zone. Future studies will investigate additional detailed isotope studies to resolve fluid-rock interaction values, and fluid temperatures.

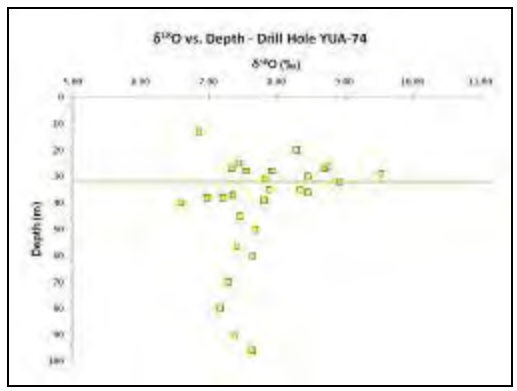

Fig. 3. Oxygen stable isotope data from drill hole YUA-74 showing an elevated δ18O envelope surrounding the main ore zone.

CONCLUSIONS

New mapping and bulk rock geochemistry of the Lac Cinquante uranium deposit has revealed a more detailed geological history than previously reported. The combination of geology and geochemistry have provided important preliminary results that will be important for understanding the metallogenesis and formation of this unconformity associated uranium deposit. Future studies at Lac Cinquante will focus on dating the mineralization, constraining the fluid temperatures and composition responsible for mineralization, and more detailed mineral chemistry of the alteration halo around the deposit.

ACKNOWLEDGEMENTS

We would like to thank Kivalliq Energy Corporation, Kaminak Gold Corporation and the Natural Sciences and Engineering Research Council of Canada for funding the project. NJB would like to thank the Society of Economic Geologists for an SEG Graduate Student Fellowship, as well as the Mineralogical Association of Canada, the University of Western Ontario Northern Research Committee and Graduate Thesis Research Awards Fund for additional research funds.

REFERENCES

BERMAN, R.G., DAVIS, W.J., & PEHRSSON, S., 2007. Collisional Snowbird tectonic zone resurrected: Growth of Laurentia during the 1.9 Ga accretionary phase of the Hudsonian orogeny. *Geology*, **35**, 911-914.

HOFFMAN, P.F., 1988. United Plates of America, the Birth of a Craton: Early Proterozoic Assembly and Growth of Laurentia. *Annual Reviews in Earth and Planetary Science*, **16**, 543-603.

MILLER, A.R., STANTON, R.A., CLUFF, & G.R., MALE, M.J., 1986. Uranium deposits and prospects of the Baker Lake Basin and subbasins Central District of Keewatin, Northwest Territories. In: Evans, E.L. (Ed.) Uranium Deposits of Canada. Canadian Institute of Mining and Metallurgy, Special Volume 33, 263-285.

RAINBIRD, R.H., HADLARI, T., ASPLER, L.B., DONALDSON, J.A., LECHEMINANT, A.N., PETERSON, T.D., 2003. Sequence stratigraphy and evolution of the Paleoproterozoic intracontinental Baker Lake and Thelon basins, western Churchill Province, Nunavut, Canada. *Precambrian Research*, **125**, 21-53.

The New Brunswick Groundwater Chemistry Atlas: a geographical representation of groundwater quality in New Brunswick

Annie E. Daigle[1], Mallory Gilliss[1], & Darryl A. Pupek[1]
[1]*New Brunswick Department of Environment, 20 McGloin St., Fredericton, NB E3A 5T8 CANADA*
(e-mail: annie.daigle@gnb.ca)

ABSTRACT: Under the Potable Water Regulation of the *Clean Water Act*, the Province of New Brunswick maintains a database of groundwater quality data collected from domestic water wells drilled since 1994. Privacy regulations prohibit the distribution of these data by any method which identifies the individual well owner or associated property. In order to make these data publicly available, the New Brunswick Department of Environment recently released the New Brunswick Groundwater Chemistry Atlas (Atlas). The Atlas was created using the results from approximately 10,500 inorganic chemistry samples collected from domestic water wells drilled between 1994 and 2007. The 28 parameters in the standard inorganic chemistry analysis conducted at the Department of Environment Analytical Services Laboratory are individually mapped in the Atlas. Each map presents the range in concentrations along with information pertaining to the distribution of the data and their relationship to applicable Health Canada drinking water quality guidelines. In addition to providing a baseline measurement of groundwater quality in the Province, the Atlas makes the information in New Brunswick's domestic water well database more accessible to the public. The geographical representation of these data facilitates trend analysis and serves as a valuable resource for many user groups, most notably health professionals, geologists, groundwater researchers, and land use planners.

KEYWORDS: *groundwater quality, domestic well logs, inorganic chemistry, database, New Brunswick.*

INTRODUCTION

Under the Potable Water Regulation of the *New Brunswick Clean Water Act*, the Province of New Brunswick maintains a database of groundwater quality data collected from domestic water wells drilled since 1994.

New Brunswick privacy regulations prohibit the distribution of these water quality data by any method which identifies the individual well owner or associated property. These data can only be provided to researchers and other interested parties in aggregate form with all identifying coordinate data removed.

In 2006, as a means of making these data available in a spatial format to various user groups, the New Brunswick Department of Environment (DENV) began development of a series of thematic maps of groundwater quality using information in the domestic water well database. The goal was to develop a series of maps, which could be publicly released without compromising privacy regulations. Based in part on the previous work done by Rivard *et al.* (2005) in the Maritimes Carboniferous Basin, the resulting New Brunswick Groundwater Chemistry Atlas (Atlas) was published in December 2008 and is available on-line at www.gnb.ca/env.

BACKGROUND

When a domestic water well is drilled in the Province of New Brunswick, the well driller completes a Water Well Driller's Report outlining the well location, construction details, estimated water yield, and geology encountered. The report is forwarded to the DENV where the information is entered into the domestic well log database.

The well owner is also given a copy of the Water Well Driller's Report and is required by law (under the *Potable Water Regulation – New Brunswick Clean Water Act*) to purchase a Water Quality Analysis

Voucher at the time of drilling. The well owner then redeems the voucher by collecting the necessary water samples, using the bottles and a methodology provided by the DENV, and submitting them to the DENV Analytical Services Laboratory for a standard inorganic chemistry analysis.

Results are entered into the DENV water quality database and a report with the results is sent to the well owner by the New Brunswick Department of Health (NB Health). A flow chart of this process is illustrated in Figure 1.

METHODOLOGY

The results of water quality analyses were extracted from the water quality database for the period of January 1, 1994 to December 31, 2006. This resulted in 10,664 usable water chemistry results, although not every parameter was analysed is each case resulting in variations in the sample size. The domestic well log database reported 20,478 usable well logs for the same time period.

The discrepancy between the number of well logs and the number of water chemistry results indicates that roughly 50% of well owners did not submit a water quality sample to the DENV for analysis and redeem their Water Quality Analysis Voucher over the reporting period.

In all 28 parameters were individually mapped: alkalinity, aluminum, antimony, arsenic, barium, boron, bromide, cadmium, calcium, chloride, chromium, conductivity, copper, fluoride, hardness, iron, lead, magnesium, manganese, nitrate, pH, potassium, selenium, sodium, sulphate, thallium, uranium, and zinc. These parameters constitute the standard inorganic analysis conducted at the DENV Analytical Services Laboratory.

Along with individual chemical parameters the Atlas also includes a plot of well depths and maps of NB surficial geology (modified from Rampton, 1984) and bedrock lithology (modified from Fyffe & Richard, 2007).

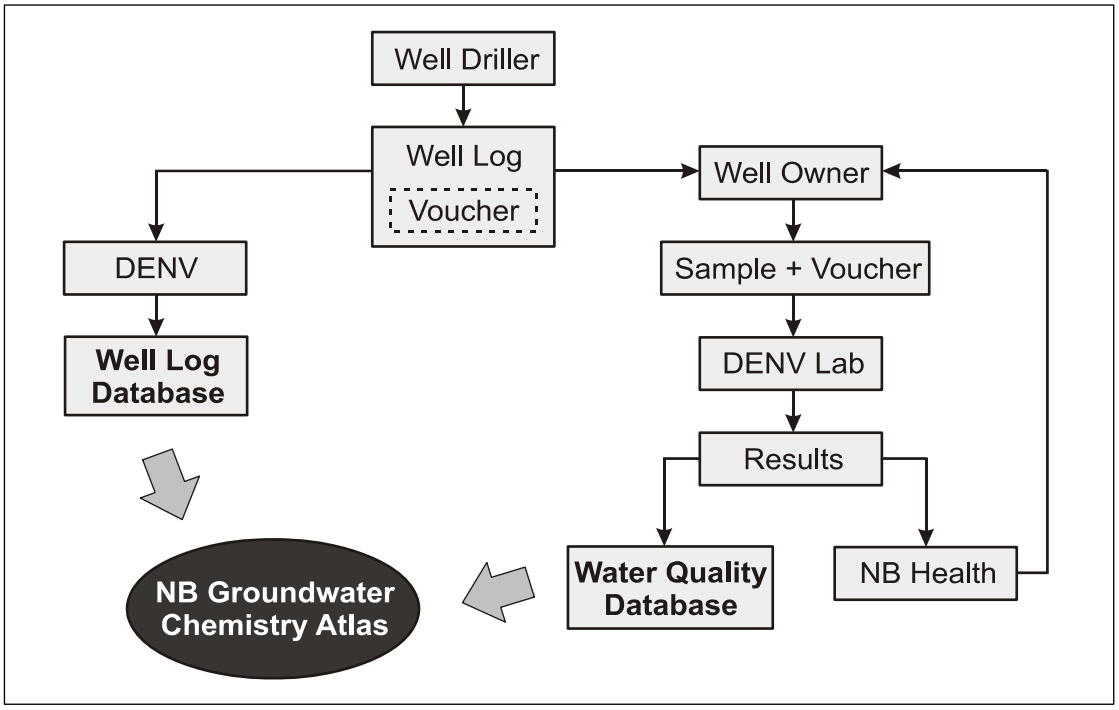

Fig. 1. Flow chart of water quality analysis voucher process for newly drilled domestic water wells in New Brunswick.

RESULTS

For each individual parameter, the Atlas plate indicates the range in concentrations of the parameter along with information pertaining to the distribution of the data and their relationship to the Health Guidelines for Canada Drinking Water Quality (Health Canada, 2008).

The following tables provide a detailed breakdown of the compliance of water well samples with health-based guidelines (Table 1) and aesthetic guidelines (Table 2). These results indicate that in general the water quality of domestic water wells in New Brunswick is very good. The most common water quality issues in New Brunswick are due to excessive iron and manganese in well water, which is attributable to the natural geology of the province.

Table 1. Compliance of samples with health-based guidelines

Parameter	Samples in compliance
Antimony	99.4%
Arsenic	94.1%
Barium	98.6%
Boron	100%
Cadmium	99.9%
Chromium	99.8%
Fluoride	95.0%
Lead	97.3%
Nitrate	99.4%
Selenium	98.9%
Uranium	97.9%

Table 2. Compliance of samples with aesthetic guidelines.

Parameter	Samples in compliance
Chloride	96.7%
Copper	99.9%
Hardness	89.2%
Iron	71.2%
Manganese	60.2%
pH	86.3%
Sodium	96.6%
Sulphate	99.4%
Zinc	99.9%

In certain instances, the Atlas indicates a relationship between a water chemistry parameter and the bedrock geology, the geological history, or general land use of the area. For example, higher concentrations of iron and manganese are encountered in the Carboniferous Basin, higher nitrate concentrations are seen in agricultural areas along the Saint John River valley, and elevated sodium and chloride can indicate areas that are vulnerable to salt water intrusion but can also outline inland areas where relic sea water from the late Quaternary is found at depth.

In the future, additional data analysis will be conducted on the dataset in order to further examine the relationships between groundwater chemistry and well depth, surficial and bedrock geology, and structural features such as fault zones.

CONCLUSIONS

Since its release in December 2008, the New Brunswick Groundwater Chemistry Atlas has proven to be a useful tool to help educate New Brunswickers about general groundwater quality in the province and identify areas with potential water quality concerns. The Atlas can be used in conjunction with other information by planners and developers to make informed decisions about land use planning and sustainable development. The data are also being used in environmental health research and mineral exploration by groundwater researchers and geologists.

The Atlas provides a basis for further research into factors that affect natural groundwater chemistry. It also serves as a baseline for comparing shifts in water quality overtime due to climatic changes and other factors.

Since the Atlas only includes water chemistry data up to December 31, 2006, it is intended to be periodically updated as additional well water quality data become available.

The Atlas should be used for general information purposes only, and independent confirmation of groundwater quality for specific sites is recommended.

ACKNOWLEDGEMENTS

The New Brunswick Groundwater Chemistry Atlas was completed under the Canada-New Brunswick Water Quality Monitoring Agreement with contributions from Environment Canada and the New Brunswick Department of Environment. Additional support was provided by the New Brunswick Department of Natural Resources and the Maritimes Groundwater Initiative of the Geological Survey of Canada. We would like to thank Rockflow Geoscience Consultants Inc., in particular Norah Hyndman, for data analysis and Jeff Stymiest of the Information Technology Branch of the New Brunswick Department of Local Government for his technical support in map development.

REFERENCES

FYFFE, L.R. & RICHARD, D.M. 2007. Lithological map of New Brunswick. *New Brunswick Department of Natural Resources*; Minerals, Policy and Planning Division. Plate **2007-18**.

HEALTH CANADA 2008. Follow: Environmental and Workplace Health, Guidelines for Canadian Drinking Water Quality, 30/05/08, http://www.hc-sc.gc.ca.

RAMPTON, V.N. 1984. Generalized surficial geology map of New Brunswick. *New Brunswick Department of Natural Resources and Energy*; Minerals, Policy and Planning Division, **NR-8**.

RIVARD, C., DEBLONDE, C., MICHAUD, Y., BOISVERT, V., CARRIER, C., CASTONGUAY, S., & LEFEBVRE, R. 2005. Hydrogeological Atlas of the South-Central Areas of the Maritimes Carboniferous Basin. *Geological Survey of Canada*, Open File **4884**, 54 p.

Spatial geochemical trends of beach and dune sands from the Northeastern coast of Mexico: implications for provenance

Juan Jose Kasper-Zubillaga[1], John S. Armstrong-Altrin[1], & Arturo Carranza Edwards[1]

1 Instituto de Ciencias del Mar y Limnologia, Universidad Nacional Autonoma de Mexico, Circuito Exterior s/n, Coyoacan, México DF, México 04510 (e-mail kasper@icmyl.unam.mx)

ABSTRACT: A geochemical analysis of major, trace and rare earth elements was carried out in beach sands collected from the Northeastern coast of Mexico in order to observe the spatial trends along three different beaches. Results show that major elements patterns along the beaches are controlled by heavy minerals and plutonic and sedimentary input towards the coast. In addition, trace elements tendencies indicate that the beach sands are influenced by the presence of magnetite. Finally, the differences in Eu anomalies indicate a mix of felsic to mafic and intermediate rocks and feldspar weathering.

KEYWORDS: *beach, sand, provenance, Mexico*

INTRODUCTION

Beach and dune sediments are compositionally controlled by physical, chemical and mechanical factors such as waves, wind, and long shore currents, climate, relief, source composition, transport and river discharges among others (Folk 1974, Ibbeken & Schleyer, 1991; Carranza-Edwards *et al*. 1994; Critelli *et al.* 1997; Carranza-Edwards *et al*. 1998; Armstrong-Altrin *et al*. 2003; Armstrong-Altrin *et al*. 2004; Kasper-Zubillaga & Carranza-Edwards 2005; Kasper-Zubillaga *et al*. 2008a). A wide range of techniques are used for geochemical determinations to investigate the compositional differences of the beach and dune sediments. Such techniques are defined by major, trace and rare earth elements analyses. Furthermore, these techniques allow to understanding the multi-factorial roles that control the composition of coastal sediments. In this paper we focus our attention in showing the spatial trends of geochemical data obtained during the dry season in the northeastern coast of the Gulf of Mexico to discuss the provenance implications.

STUDY AREA

The study area is located in the coastal area of the state of Tamaulipas, Mexico (22°10' 24°00'W; 98°00'N).The sampling was carried out in three main localities: Playa Miramar, Boca del Tordo and La pesca (Figs. 1&2).

Main rivers discharging in each site are Panuco, Carrizal and Soto La Marina.

The geology of the study area comprises mainly: limestones, shales, alluvial deposits and basic extrusive and intrusive rocks.

MATERIALS AND METHODS

Sand samples were dried at 110 °C and treated with lithium meta and tetraborate to make pressed powder pellets. They were analysed using a X-ray fluorescence Siemens SRS3000 equipment for major and trace elements. For major and trace elements precision is valuated in terms of relative standard deviation being $<$ 1% (Sutarno & Steger 1985).

The REE analysis was carried out in twenty two sand samples by using 0.1 g of dried sample (mesh 200) and digested with strong acid. Digestion was performed in teflon vessels using 4 ml of HCl O_4 and 10 ml HF. This mixture was heated and residue dissolved in distilled water.

Residue was incorporated to a volumetric flask. Determinations of REE were carried out with an ICP mass spectrometer VG Elemental model PQ3. Detection limits were calculated as the concentration equivalent to three times the standard deviation of five replicates of the blank

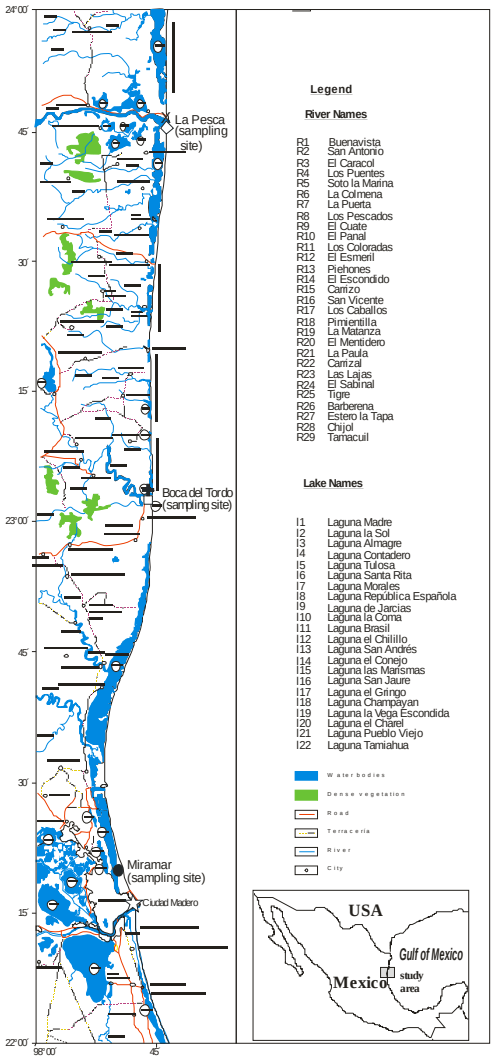

Fig. 1. Study area and sampling sites.

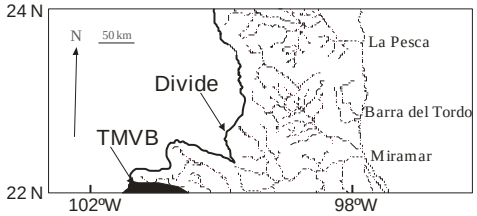

Fig. 2. Map of showing the Trans-Mexican Volcanic Belt (TMVB) near to the study area.

solution. It was better than 200ppt for all elements determined. Calibration of the apparatus was done with a 0.1, 1 10 and 100 ppb multi elemental standard solution (SPEX- High Purity) and a blank solution of de-ionized water all containing HNO3 at 2%. Results were observed for international standards (JG-2). The validity of the analytical procedure was assessed by means of accuracy and precision tests. They were calculated by comparing measured and reference values (JA-2). All elements determined had a better than 10 % relative standard deviation (RSD) precision. Data resulted for BCU-3 or "in house standard indicated good agreement with the certified values.

Chondrite-normalized REE patterns were based on values by Evensen *et al*. (1978) averaging the samples firstly determined in ppm for each site.

RESULTS & DISCUSSION

From Figure 3 it can be observed that among the major element trends Ti shows various peaks from localities 10 to 22 that correspond to some beach areas from Playa Miramar, the whole area of Boca del Tordo and one sample from the La Pesca This suggests that this area might have influenced by heavy minerals and plutonic and sedimentary outcrops as it has previously reported in dune sands from Mexico (Kasper-Zubillaga *et al*. 2008a). The rest of the major elements do not show differences in their trends along the coast. However, Ca shows a dynamic behavior represented by oscillations along the coast probably produced by the amount of biogenic debris.

Trace elements show that V exhibit high peaks in Boca del Tordo beach probably associated with the presence of some heavy minerals like magnetite (Kasper-Zubillaga *et al*. 2008a).

Rare earth elements patterns show differences in Eu anomalies for the samples studied from Boca del Tordo (Fig. 5) that can be attributed to the mix of felsic and mafic sources. This variation can also be explained due to the impoverishment of feldspars due to weathering (Kasper-Zubillaga *et al*. 2008b). Also Boca del

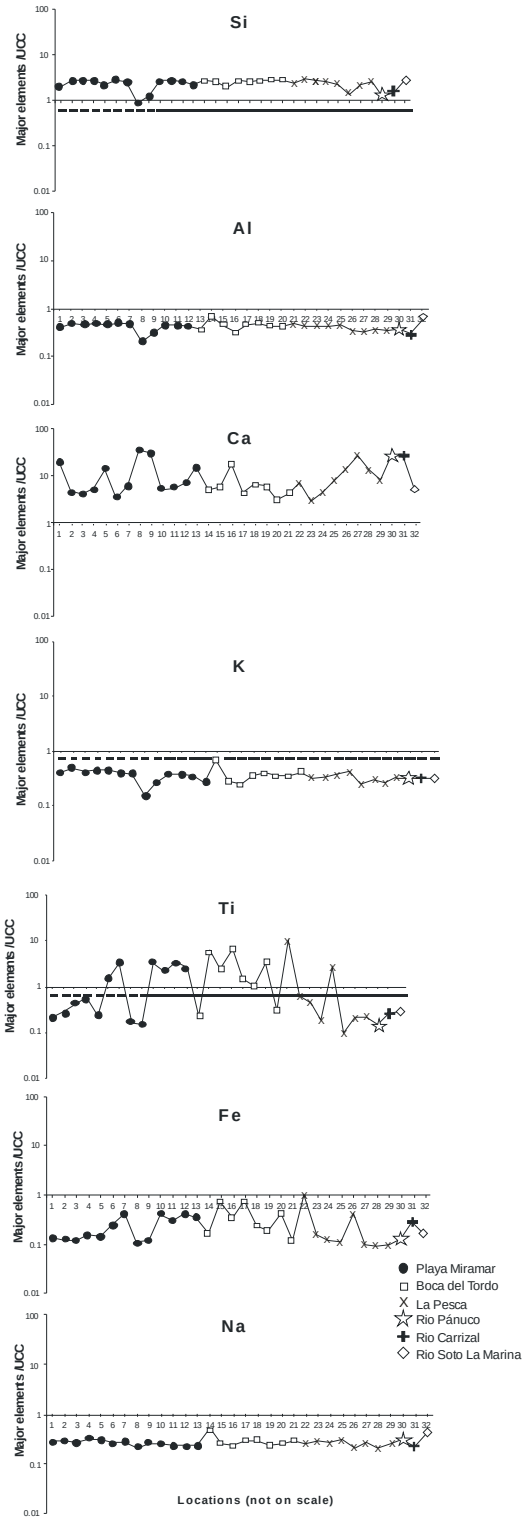

Fig. 3. Spatial trends of major elements at beach and dune sands from the northeastern coast of Mexico.

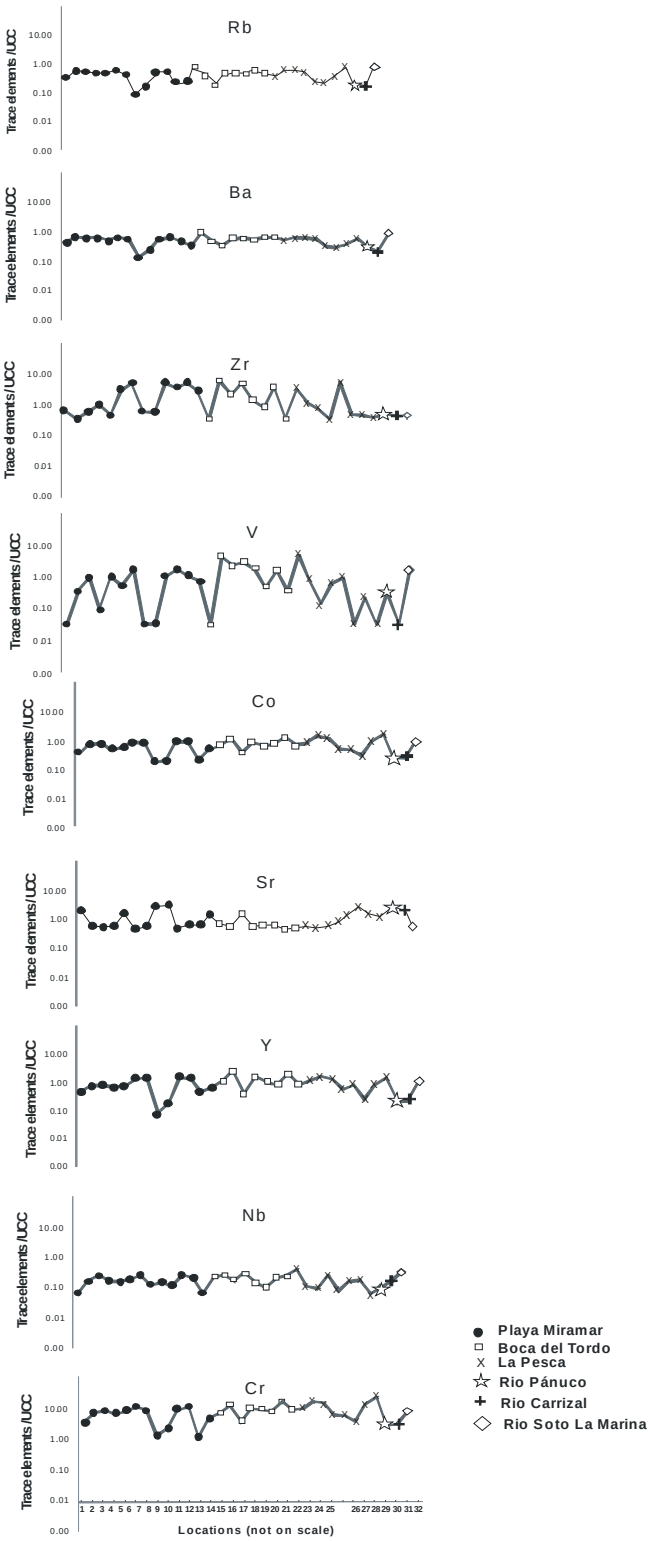

Fig. 4. Trace elements tendencies along the northeastern coast of Mexico.

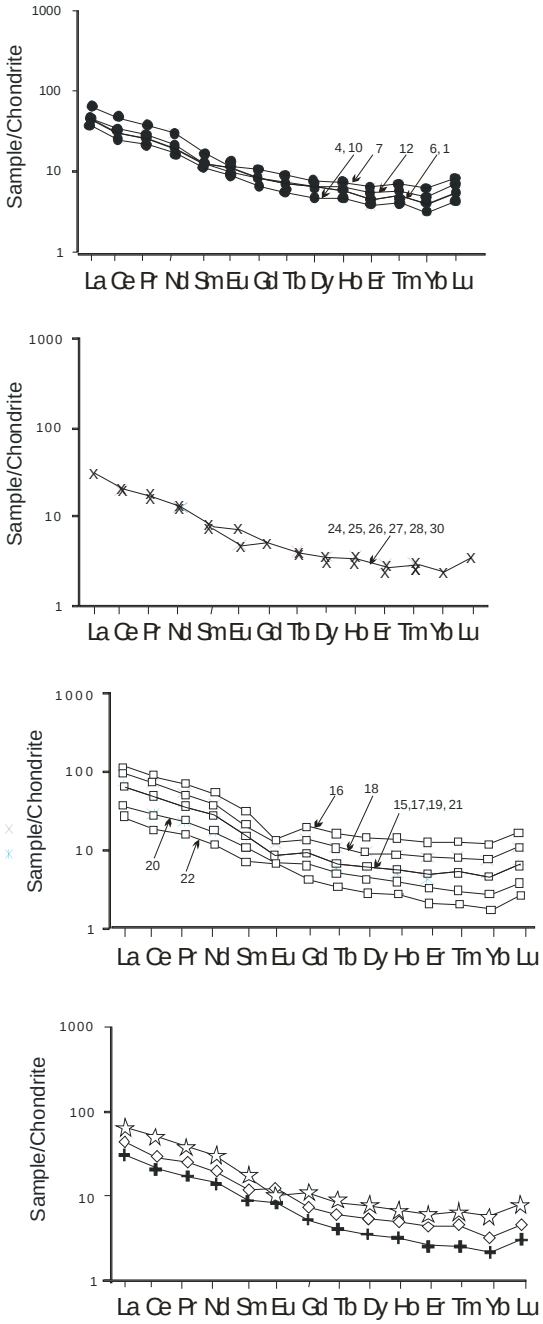

Fig. 5. Rare earth elements in the northeastern coast of Mexico.

Tordo concentrates more rare earth elements especially in samples 16 and 18 which is probably due to the presence of some heavy minerals that are potential carriers of rare earth elements (Kasper-Zubillaga *et al*. 2008b). The possible source of volcanic is mainly through the Panuco River that intersects volcanic from the Trans-Mexican Volcanic Belt.

CONCLUSIONS

(1) Major elements trends show that Northeastern Mexican beaches are influenced by heavy minerals and plutonic and sedimentary outcrops.

(2) Trace elements tendencies suggest that the Boca del Tordo beach is more influenced by the presence of magnetite than other beaches.

(3) Rare earth elements trends show a negative and positive Eu anomalies in some samples studied from the Northeastern beaches suggesting a mix of felsic and mafic source rocks and feldspar weathering.

ACKNOWLEDGMENTS

We are indebted to Rufino Lozano and Ofelia Morton for the geochemical analyses carried out at the Instituto de Geologìa and Instituto de Geofisica respectively from the Universidad Nacional Autònoma de Mexico, Mexico.

REFERENCES

ARMSTRONG-ALTRIN, J.S., VERMA, S.P., MADHAVARAJU, J., LEE, Y.I., & RAMASAMY, S. 2003. Geochemistry of upper Miocene Kudankulam limestones, southern India. *International Geological Review,* **45**, 16-26.

ARMSTRONG-ALTRIN, J.S., LEE, Y.I., VERMA, S.P., & RAMASAMY, S. 2004. Geochemistry of sandstones from the Upper Miocene Kudankulam Formation, Southern India: implications for provenence, weathering and tectonic setting. *Journal of Sedimentary Research*, **74**, 285-297.

CARRANZA-EDWARDS, A., ROSALES-HOZ, L., & SANTIAGO-PÉREZ, S. 1994. Provenance memories and maturity of holocene sands in Northwest Mexico. *Canadian Journal of Earth Sciences*, **31**, 1550-1556.

CARRANZA-EDWARDS, A., BOCANEGRA-GARCIA, G., ROSALES-HOZ, L. & DE PABLO GALÁN, L. 1998. Beach sands from Baja California Peninsula, México. *Sedimentary Geology*, **119**, 263-274.

CRITELLI, S., LE PERA,, E., & INGERSOLL,R.V. 1997.The effects of source lithology, transport, deposition and sampling scale on

the composition of southern California sand. *Sedimentology*, **44**, 653-671.

EVENSEN, M.N., HAMILTON,P.J., & ONIONS.P.K., 1978.Rare earth abundance in chondrite meteorites. *GeochimIca et. Cosmochimica Acta*, **42**, 1199-1212.

FOLK, R. L., 1974.Petrology of Sedimentary Rocks. *Hemphill Publishing Co., Austin, TX*.

IBBEKEN, H. & SCHLEYER, R., 1991.Source and Sediment. *Springer Verlag. Berlin*.

KASPER-ZUBILLAGA, J.J. & CARRANZA-EDWARDS, A., 2005.Grain size discrimination between sands of desert and coastal dunes from northwestern Mexico. *Revista Mexicana de Ciencias Geológicas,* **22**, 383-390.

KASPER-ZUBILLAGA, J.J., ACEVEDO-VARGAS, B., MORTON-BERMEA, O., & ORTIZ-ZAMORA, G., 2008a, Rare earth elements of the Altar Desert dune and coastal sands, Northwestern Mexico. *Chemie Der Erde Geochemistry*, **68**, 45-69.

KASPER-ZUBILLAGA, J.J., CARRANZA-EDWARDS, A., & MORTON-BERMEA, O. 2008b.Heavy minerals and rare earth elements in coastal and inland dunes of El Vizcaino Desert Baja Califonia Peninsula, Mexico. *Marine Georesources and Geotechnology*, **26**, 172-188.

SUTARNO, R. & STEGER, H.F., 1985.The use of certified reference materials in the verification of analytical data and methods. *Talanta*, **32**, 439-445.

Biogeochemistry of Iron

A.L. Kovalevskii[1] & O.M. Kovalevskaya[1]
[1]*Geological Institute Siberian Branch of Russian Academy of Sciences Sakhyanova Street, 6a, Ulan-Ude-47, 670047 RUSSIA (e-mail: koval@gin.bscnet.ru)*

ABSTRACT: 9070 samples of plants and 1060 samples of soils, rocks and iron ores were studied when research was done on four iron ore deposits. This allowed for the first time to get a considerable volume of fact data about the iron accumulation by a large number of studied bioobjects of plants not only in Angaro-Ilimskii iron ore region, but also in other regions of the East Siberia, particularly in Buryatia and Chita area. The main result of the research is revealing the System of Nonbarrier-Barrier Accumulation (SNBBA) of plants and external layers of bark of trunks of various species of trees as bioobjects, nonbarrier in relation with iron.

Keywords: *biogeochemistry, plants, iron, beryllium, nonbarrier-barrier*

INTRODUCTION

The objects of biogeochemical researches were four iron-ore deposits of Angaro-Ilimsk ore-bearing region of Irkutsk area: Rudnogorskoe, Oktyabr'skoe, Tat'yaninskoe and Zmeinogorskoe. All deposits are explosion tubes of rounded and oval form. Magnetite and seldom gematite iron-ore bodies, which are of practical interest, have mainly ring-shaped, seldom secant, linear form on them. Ring-shaped ore bodies are situated on peripheries of explosion tubes. Their thickness is measured by meter and tens of meters, iron content changes from 20 to 60 % and on average is close to 30-35%. Explosion tubes break through Ordovician and Cambrian sedimentary rocks and are of Triassic age. On their contacts with carbonate rocks the complex processes of scarning are widely developed.

THE SYSTEM OF NONBARRIER-BARRIER ACCUMULATION (SNBBA) OF PLANTS IN RELATION TO IRON

The first data about nonbarrier iron accumulation by external layers of tree trunk bark were received by us on Ermakovskii fluorite-beryllium deposit in Zabaikalye. Detailed research of chemical element (CE) distribution in cross-sections of trees trunks and in their other parts and species of plants were conducted here for the first time, the aim of which was – SNBBA of plants in relation with beryllium and companions of its deposits (Kovalevskii & Kovalevskaya, 1979). Here suddenly it was established that over a fluorite-beryllium ore body, the average content of iron for four specimens were anomalously high. In the external layer of pine trunk bark it was 4.1 %, in subereous cones and roots – 5 %. These contents in nonbarrier bioobjects of pine were higher than in soils (2 % in horizon A, 3 % in B, and 1 % in C). For these nonbarrier bioobjects plant-soil coefficient (PSC) of iron were unusually high 2-2.5. According to Perel'man (1989), iron is referred to the elements of average and weak biological capture with the coefficients of biological absorption (CBA=PSC) 0,n – 0,0n. Minimal content of iron at the considered key point of Ermakovskii beryllium deposit – 0.8 % was established in bast (cambiums) of pine with the contents in twigs, needles and green cones equal to1.2; 2.1 and 1.4 %. For given four barrier bioobjects PSC were received equal to 0.4; 0.6; 1.0; 0.7 considering an average iron content in soil equal to 2 % – considerably less, than its clark, which was equal approximately to 5 %. Established high PSC of iron on beryllium deposits are connected with pyrite form of iron in fluorite-beryllium ores containing to 50-70 % of fluorite. On this beryllium

deposit, it was established that iron like Be, F, Li, Pb, Zr, Ti, Si, Al, `has the highest relative concentrations in external layers of tree trunk bark in comparison with other layers of bark, noticeably (in 2.5 – 4 times) enriches the small fraction of crushed pine and larch bark and forms its own minerals in the bark: pyrite, magnetite (?) and ilmenite. These data were completely confirmed and supplemented when biogeochemistry of iron on its deposits in Angaro-Ilimskii ore region was researched.

Iron in cross-sections of larch, pine, birch, cedar, fir tree, rowan-tree trunks turned out to be distributed in the same type (Fig. 1). For all studied species of trees the maximal contents of iron in the external layer of bark, and minimal – in internal layer of the youngest bast cells consisting mainly of dividing cambial cells were established. For all species of trees in 1.5-2 times greater content of iron is established in “young” sap-wood in comparison with “old” nucleous wood in the central part of trunk. According to concentration curves (Fig. 2) in the system: “external layers of trunks bark – other bioobjects of the same species of trees” and comparison of iron contents in various species and parts of plants on the most intensive biogeochemical haloes of iron 213 studied bioobjects of plants were

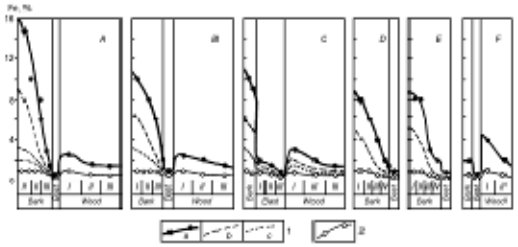

Fig. 1. Distribution of iron in trees trunk on the background and the haloes of iron ore bodies (deposit Oktyabr’skoe, Tat’yaninskoe, and Zmeinaya gorka). A – larch (*Larix dahurica* Turcz.); B – pine (*Pinus silvestris* L.); C – birch (*Betula platyphylla* Sukacz.); D – cedar (*Cedrus sibirica* (Rupr.); E – fir-tree (*Picea obovata* Ledeb); F – rowan-tree (*Sorbus sibirica* Hedl.). 1 – on the haloes (a – the most intensive, b – of middle intensive, c – the less intensive); 2 – on the background.

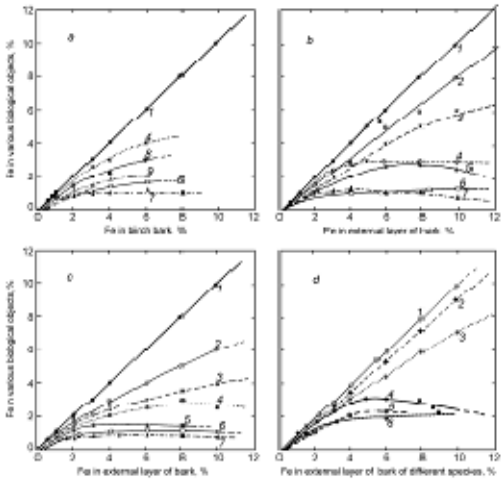

Fig. 2. Concentration dependence in the system: the known nonbarrier biological object – the studied biological object for iron on the Oktyabr’skoe iron ore deposit.
a – birch: 1 – bark, 4 – sap-wood, 6 – nucleus wood, 7 – bast, 8 – leaves, 9 – twigs.
b – larch: 1 – external layers bark, 2 – middle layers of bark, 3 – internal layers of bark, 4 – sap-wood, 5 – twigs with needles, 6 – nucleus wood, 7 – bast.
c – pine: 1 – external layers of bark, 2 – average layers bark, 3 – internal layers bark, 4 – sap-wood, 5 – twigs with needles, 6 – nucleus wood, 7 bast.
d – external layers of bark of different species: 1 – of larch, 2 – of pine, 3 – of birch, 4 – of cedar, 5 – of fir-tree, 6 – of aspen.

grouped for the first time according to their prospecting informativeness to this chemical elements (Kovalevskii, 1991).

From 213 studied bioobjects overgroung bioobjects of plants – external layers of trunks layers of trunks bark and Siberian larch and ordinary pine stumps, their suberificated cones and birch bark and also roots of all studied species of trees: larch, pine, and birch and green moss are mostly informative. Iron concentrations in their ash on its most intensive haloes exceed 10% according to data of the spectral analyses and reach 12-16% according to data of X-ray-radiometric and chemical analyses. In these 16 (7% of 213 studied) most informative bioobjects haloe concentrations of iron exceed the background in 5-20 times, which approximately corresponds to contrast of

primary lithogeochemical haloes of iron in its ore bodies. That is why these biological objects can be considered nonbarrier, quantitatively-informative in relation to iron. They, first external layers of bark of larch, pine, cedar and fir tree trunks and also birch bark, are recommended for various researches of iron biogeochemistry. Especially if it concerns iron is used as element-indicator of magnetite ores and also of pyritization and sideritization zones, iron of which is more available to plants in comparison with iron of magnetite ores.

RELATIVE CONTENT OF IRON IN VARIOUS BIOLOGICAL OBJECTS (BIOOBJECTS) OF PLANTS (RCBO)

The second quantitative parameter, necessary for interpretation of received biogeochemical data is relative content of iron in bioobjects selected on the same points of observation – RCBO. Meanings of RCBO established for bioobjects of the studied iron ore deposits show inconsiderable differentiation between them exceeding ± 20% (Table 1).

Table 1. Relative content (RCBO) of iron in bioobjects recommended for biogeochemical researches for this element.

Biological objects	Iron ore deposits			Ave-rage
	Oktya-b'rskoe	Tat'ya-ninskoe	Zmei-naya gorka	
Trunks bark:				
pine (standard)	1,0	1,0	1,0	1,0
larch	1,1	1,1	1,1	1,1
cedar	1,2	1,3	1,1	1,2
fir tree	0,9	1,0	0,9	0,9
birch	0,8	0,9	0,8	0,8
Suberificated cones:				
pine	1,1	1,1	1,2	1,1
larch	1,2	1,3	1,1	1,2
fir tree	0,7	1,3	0,8	0,9
Young underwood of pine	0,7	0,9	0,8	0,8

INTENSITY OF BIOLOGICAL ABSORPTION OF IRON

On all four studied iron ore deposits and on all other key sites the data of which were used in this report, iron absorption by plants take place according to lithobiogeochemical model (Kovalevskii, 1991). According to this model there are no free ground waters in the rootinhabited zone, and chemical elements (CE) are absorbed only from its solid phase. Intensity of biological absorption in this case is determined with the help of plant-soil (PSC) and plant-rock (PRC) coefficients. During last years PRC was introduced by us for conditions, characteristic for vein ore deposits. On them often the horizon of plant nutrition, which is determined according to special methodics (Kovalevskii, 1991), of the studied CE turned out to be arranged to the lowest soil horizon D – elluvium of bedrocks.

We determined PSC of CE as its contents ratio in ash of nonbarrier plant bioobject and in soil on the horizon of its nutrition, that is of great significance for easily-mobile chemical elements, which often enrich lower and rarely upper (nitrogen, phosphorus, manganese) soil horizons. For watershare elluvium landscapes essential differentiation of iron contents in soil sections wasn't observed. For slope landscapes over not thick iron ore bodies depletion of upper soil horizons was observed due to their horizontal displacement concerning eluvium. Therefore is why also as for other ore elements we used usually the lower soil horizon C at the standard depth of our soil sections 0,8-1 m to calculate PSC.

According to data we have values of PSC depend on mineral and chemical forms of the studied CE. The main ones are dependence on solubility of minerals and size of their grains. Four main forms of iron in soils: magnetite (main), gematite, pyrite and isomorphic (non-mineral) were studied by us. Easily soluble siderite (carbonate) form of iron is of great interest, but in the studied conditions such iron ores known on Ozernyi pyrite-polymetal deposit were oxidized to the significant depth and converted into hydroxide forms in the rootinhabited zone.

On all studied by us iron ore deposits in Baikal-Amur main line (BAM) region magnetite iron dominates in ores. Only on Oktyabr'skii deposit hematite-magnetite

ore bodies are known. Magnetite ores have various structure, texture and size of grains that was displayed in intensity of iron absorption by nonbarrier bioobjects of plants. The most disperse hardly enriched magnetite was found on Tat'yaninskii deposit. Biogeochemical anomalies of iron in nonbarrier bioobjects, which are here external layers of bark (crust) of pine, larch and birch trunks correspond well to iron ore bodies. At background contents of iron in trees bark ash 0.4-1,6 %, but in soils – 2-8%, its PSC on the background was equal to in average 0,2. Over iron ore bodies with concentrations 25-45 % biogeochemical anomalies of iron with its concentrations in ash of nonbarrier bioobjects 10-16 % at average value of PSC=0.3 were established, i.e., here availability of iron of disperse magnetite to plants was in 1.5 times higher than on the background, that is very favourable when using iron anomalies in plants for iron ore mineralization indication.

On the Oktyabr'skii deposit biogeochemical anomalies of iron are characteristic not for all known ores. Such anomalies were not revealed over dominating here massive gematite-magnetite ore bodies that evidenced inaccessibility to plants of iron being in composition of gematite and massive magnetite. Average PSC of iron over gematite-magnetite ore bodies were made 0.01-0,02 at its contents in birch, pine and larch bark 0.2-1.0 %, which were not different from background contents, and in gematite-magnetite ores – 25-55 %. Biogeochemical anomalies of iron with its contents 3-7 % reaching 8-10 % were observed over various varieties of magnetite ores with contents 25-45 %. PSC of iron is here 0.1-0.4; approximately in 20 times higher than over massive gematite-magnetite ores. Over disperse magnetite ores of Oktyabr'skii deposit the average values of PSC of iron were the same as on Tatyaninskii deposit and were 0.3-0.4. Unexpectedly four mostly intensive biogeochemical anomalies with 7-12 % iron were revealed outside the known iron ore bodies. These anomalies appeared to be connected with three zones of pyritization and chalcopyritization inside the diatreme and with one zone of pyritization outside its limits. When iron contents in these zones are 5-7 %, its PSC over zones of pyritization is 1.4-1.7, in average 1.5. So, on Oktyabr'skii iron ore deposit for the first time a precise dependence of PSC of iron on its three mineral forms was established. Minimal PSC over massive gematite-magnetite ores (0.01-0.02), when there are no biogeochemical anomalies, evidence practical inaccessibility of gematite and massive magnetite to plants. Average PSC = 0.1-0.4 correspond to ores with disperse magnetite, and maximal 1.4-2.5, in average 2 – to zones of pyritization, i.e., sulphide forms of iron in the root inhabited zone. For sites with non-mineral, isomorphic forms of iron, typical for the background, an average PSC = 0.2 when its contents in ash of nonbarrier bioobjects 0.5-1 %, and in soils – 3-6 % at clark close to 5 %.

CONCLUSIONS

(1) Received data evidence that iron, like the majority of chemical elements, is characterized by nonbarrier accumulation in suberificated tissues of trees, in particular, in external layers of trunk bark.

(2) Availability of iron to plants according to the lithobiogeochemical model of root nutrition depending on to its mineral forms in the root inhabited zone changes in 10-100 times.

REFERENCES

KOVALEVSKII, A.L. 1991. Biogeochemistry of plants. *Novosibirsk: Nauka*. (In Russian).

KOVALEVSKII, A.L. & KOVALEVSKAYA, O.M. 1979. Biogeochemical prospecting for beryllium deposits. *Novosibirsk: Nauka*. (In Russian).

PEREL'MAN, A.I. 1989. Geochemistry. *Moscow: Visshaya shkola.* (In Russian).

Correlation of atmospheric soil and atmospheric lead in three North American cities: can re-suspension of urban lead contaminated soil be a major source of urban atmospheric lead and cause seasonal variations in children's blood lead levels?

Mark Laidlaw[1]
[1]*4 Birch Drive, Hamlyn Terrace, NSW, 2259 AUSTRALIA (e-mail: markas1968@gmail.com)*

ABSTRACT: Soils in older cities are highly contaminated by lead from past use of lead in leaded gasoline and due to the use of lead in exterior paints. In this study the temporal variations in atmospheric soil and atmospheric lead in three North American cities are examined. This study tested the hypothesis that atmospheric lead and atmospheric soil concentrations obtained from the Interagency Monitoring of Protected Visual Environments (IMPROVE) exhibit statistically significant correlations in three North American cities. Results indicate that atmospheric soil and atmospheric lead were correlated in Detroit between November 2003 to July 2005 ($r = 0.47$, $p = < 0.001$); In Pittsburgh between April 2004 to July ($r = 0.40$, $p < 0.001$); and in Birmingham between May 2004 to December 2006 ($r = 0.35$, $p <0.001$). The hypothesis that atmospheric soil and atmospheric lead follow seasonal patterns with highest concentrations during the summer and/or autumn could not be rejected. It is suggested that atmospheric lead and atmospheric soil concentrations are correlated due to re-suspension of urban lead contaminated soils. It is further suggested that in order to decrease urban atmospheric lead concentrations, lead deposition, and children's seasonal exposure via hand to mouth activity, urban lead contaminated soils should be remediated or isolated.

KEYWORDS: *lead, soil, re-suspension, blood, poisoning, children*

INTRODUCTION

In the USA, motor vehicles used gasoline containing tetramethyl and tetraethyl Pb additives from the 1920s to 1986. By the 1950s, Pb additives were contained in virtually all grades of gasoline. By 1986, when leaded gasoline was banned, 5–6 million metric tons of Pb had been used as a gasoline additive, and about 75% of this Pb was released into the atmosphere (Chaney & Mielke 1986; Mielke & Reagan 1998). Thus, an estimated 4–5 million tons of Pb has been deposited into the US environment by way of gasoline-fueled motor vehicles (Mielke 1994). Accumulation of soil Pb created by leaded gasoline is proportional to highway traffic flow (Mielke *et al*. 1997).

In the 1970s, the presumed dominant source of soil Pb contamination was Pb-based house paint (Ter Haar and Aronow, 1974). A subsequent study of garden soils conducted in metropolitan Baltimore, Maryland, began to raise questions about that assumption. Soil around Baltimore's inner city buildings, predominantly unpainted brick, exhibited the highest amounts of Pb, and soils outside of the inner city, where buildings were commonly constructed with Pb-based paint on wood siding, contained comparatively low amounts of Pb, suggesting that Pb based house paint could not account for the observed pattern of soil Pb (Mielke *et al*. 1983). The same pattern was also found in Ottawa, Canada (Ericson & Mishra 1990).

The quantity and distribution of soil Pb have been studied in numerous places in North America (see Laidlaw & Filippelli, 2008). All these North American cities exhibited the same distance decay characteristic of high soil Pb contamination in the inner city and decreasing contamination toward the outer parts of the city as initially identified in garden soils of Baltimore (Mielke *et al*. 1983). Further, similarities in this distance decay pattern of soil Pb supports the idea

that Pb-based house paint was not the sole source contributing to these observed differences.

Soil lead concentrations have been observed to be associated with children's blood lead concentrations using multiple study designs – cross-sectional, ecological spatial, ecological temporal, prospective soil removal and isotopic (Laidlaw & Filippelli, 2008).

Average monthly blood Pb (BPb) values of children from urban areas tends to increase significantly in summer months (Haley & Talbot 2004; Laidlaw *et al.* 2005; Yiin *et al*. 2000). Early work by Mielke *et al*. (1992), Johnson & Bretsch (2002), and Johnson *et al*. (1996) suggested that blood Pb seasonality may be related to the interaction between climate and Pb contaminated soils. Yiin *et al*. (2000) actually measured seasonal changes in dust Pb levels and correlated blood Pb levels with seasonal dust Pb concentrations. Yiin *et al*. (2000) conducted a study to examine seasonal changes in residential dust Pb content and its relationship to blood Pb in preschool children. The study found that windowsill wipe samples were most correlated with blood Pb concentration and the variation of dust Pb levels for floor Pb loading, windowsill Pb loading, and carpet Pb concentration were consistent with the variation of blood Pb levels, showing the highest levels in the hottest months of the year (June, July, and August).

Laidlaw & Filippelli (2008), Laidlaw *et al*. (2005), and Filippelli *et al*. (2005) have demonstrated that seasonal variations in children's blood lead levels in Syracuse, Indianapolis and New Orleans could be predicted using soil moisture and atmospheric variables suggesting that re-suspension of urban soils contaminated by past use of leaded gasoline and paint were causally related to seasonal variations in blood lead. These papers concluded that urban lead contaminated soil was being re-suspended when soils were dry in the summer and autumn when evapotranspiration is maximised. Their assumption that soil lead is being re-suspended and is responsible for a large portion of the lead in the atmosphere is supported by lead isotopic analysis of atmospheric lead in Yerevan Armenia (Kurkjian *et al*. 2001), which indicated that following elimination of the use of lead in gasoline, 75% of atmospheric lead in the Yerevan atmosphere was derived from re-suspended soil.

Soil resuspension has the capability of entraining significant volumes of Pb into the air of urban areas. Harris & Davidson (2005) calculated that resuspension of soil is responsible for generating 54,000 kg of airborne Pb each year in the South Coast Air Basin of California (SOCAB) and will remain a major source well into the future. Similarly, Lankey *et al*. (1998) concluded that 43% of Pb emissions in the South Coast Air Basin in California resulted from the resuspension of soil and road dust.

In this study, data from Birmingham, Alabama; Pittsburgh, Pennsylvania; and Detroit, Michigan were selected to assess seasonal patterns and assess seasonal relationships between atmospheric soil and atmospheric lead.

The following hypotheses were tested:

3) Atmospheric air lead and atmospheric soil concentrations exhibit statistically significant correlations in three major North American Cities; and
4) Atmospheric soil and atmospheric lead follow seasonal patterns with highest concentrations during the summer and/or autumn.

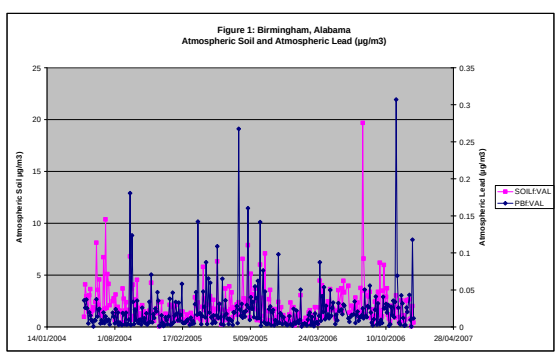

Fig. 1. Plot of atmospheric soil and atmospheric lead in Birmingham, Alabama ($r = 0.35$, $p < 0.001$).

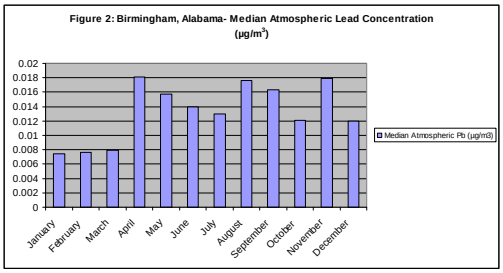

Fig. 2. Median atmospheric lead concentrations at IMPROVE air monitoring station in Birmingham, Alabama (May 2004 to December 2006).

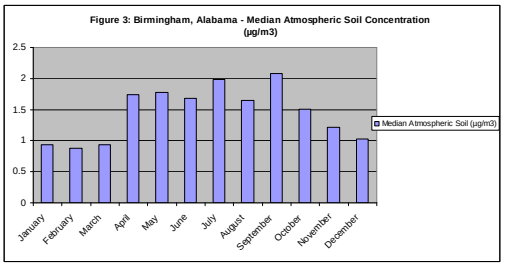

Fig. 3. Median Atmospheric soil concentrations at IMPROVE air monitoring station in Birmingham, Alabama (May 2004 to December 2006).

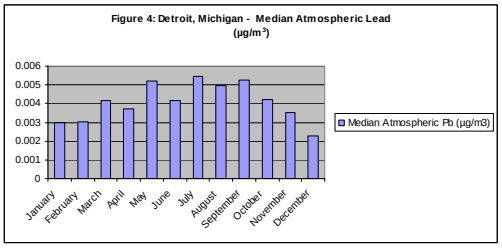

Fig. 4. Median atmospheric lead concentrations at IMPROVE air monitoring station in Detroit, Michigan (November 2003 to July 2005).

CONCLUSIONS

1) In order to decrease urban atmospheric lead concentrations, lead deposition, and subsequent children's exposure via hand to mouth activity, urban lead contaminated soils should be remediated or isolated.

REFERENCES

CHANEY, R.L. & MIELKE, H.W. 1986. Standards for soil Le ad limitations in the United States.

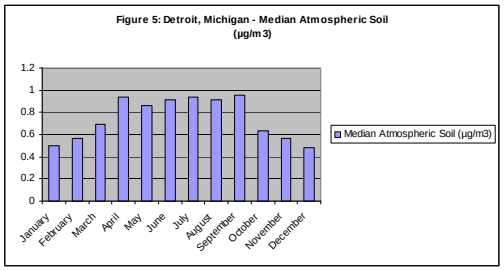

Fig. 5. Median Atmospheric soil concentrations at IMPROVE air monitoring station in Detroit, Michigan (November 2003 to July 2005).

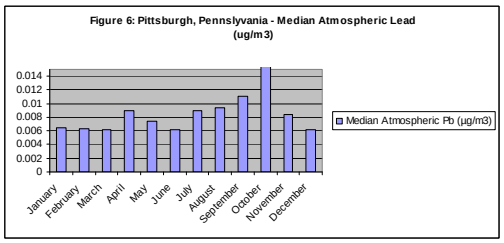

Fig. 6. Median atmospheric lead concentrations at IMPROVE air monitoring station in Pittsburgh, Pennslyvania (April 2004 to July 2005).

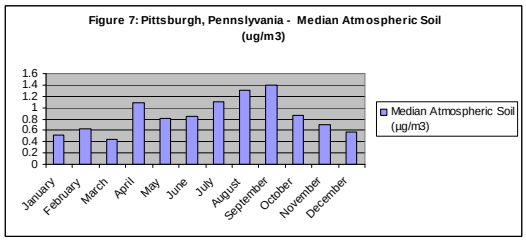

Fig. 7. Median Atmospheric soil concentrations at IMPROVE air monitoring station in Pittsburgh, Pennslyvania (April 2004 to July 2005).

In: HEAMPHILL, D.D. (ed) Trace Substances in2036 M.A.S. Laidlaw, G.M. Filippelli / Applied Geochemistry 23 (2008) 2021–2039 Environmental Health, University of Missouri, Columbia, 357–377.

Ericson, J.E. & Mishra, S.I., 1990. Soil lead concentrations and prevalence of hyperactive behavior among school children in Ottawa, Canada. Environ. Internat. **16**, 247–256.

FILIPPELLI, G.M., LAIDLAW, M., LATIMER, J., & RAFTIS, R. 2005. Urban lead poisoning and

medical geology: an unfinished story. *GSA Today*, **15**, 4-11.

HALEY, V.B. & TALBOT, T.O. 2004. Seasonality and trend in blood lead levels of New York State children. *BMC Pediatrics*, **4**, 8.

HARRIS, A. & DAVIDSON, C. 2005. The role of resuspended soil in lead flows in the California south coast air basin. *Environmental Science Technology*, **39**, 7410–7415.

IMPROVE (Interagency Monitoring of Protected Visual Environments), 2007. Available: http://vista.cira.colostate.edu/improve/. Accessed [15 November 2007].

JOHNSON, D. & BRETSCH, J. 2002. Soil lead and children's BLL Levels in Syracuse, NY, USA. *Environmental Geochemistry and Health*, **24**, 375-385.

JOHNSON, D., MCDADE, K., & GRIFFITH, D. 1996. Seasonal variation in pediatric blood levels in Syracuse, NY, USA. *Environmental Geochemistry and Health*, **18**, 81-88.

KURKJIAN R., DUNLAP, C., & FLEGAL, R. 2001. Lead isotope tracking of atmospheric response to post-industrial conditions in Yerevan, Armenia. *Atmospheric Environment,* **36**, no. 8, 1421-1429.

LAIDLAW, M.A.S., MIELKE, H.W., FILIPPELLI, G.M., JOHNSON, D.L., & GONZALES, C.R., 2005. Seasonality and children's blood lead levels: developing a predictive model using climatic variables and blood lead data from Indianapolis, Indiana, Syracuse, New York, and New Orleans, Louisiana (USA). *Environmetnal Health Perspectives*, **113**, 793–800.

LAIDLAW, M.A. & FILIPPELLI, G.M. 2008. Resuspension of urban soils as a persistent source of lead poisoning in children: A review and new directions. *Applied Geochemistry,* **23**, no 8, 2021-2039.

LANKEY, R.L., DAVIDSON, C.I., & MCMICHAEL, F.C. 1998. Mass balance for lead in the California south coast air basin: an update. *Environmental Research*, **78**, 86–93.

MIELKE, H.W., ANDERSON, J.C., BERRY, K.J., MIELKE JR., P.W., CHANEY, R.L., & LEECH, M. 1983. Lead concentrations in inner-city soils as a factor in the child lead problem. *American Journal of Public Health*, **73**, 1366–1369.

MIELKE, H.W., 1994. Lead in New Orleans soils: new images of an urban environment. *Environmental Geochemistry and Health*, **16**, 123–128.

MIELKE, H.W. & REAGAN, P.L., 1998. Soil is an important pathway of human lead exposure. *Environmental Health Perspectives*, **106**, 217–229.

MIELKE, H.W., DUGAS, D., MIELKE JR., P.W., SMITH, K.S., SMITH, S.L., & GONZALES, C.R., 1997. Associations between soil lead and children's blood lead in urban New Orleans and rural Lafourche Parish of Louisiana. *Environmental Health Perspectives,* **105**, 950–954.

YIIN, L.M., RHOADS, G.G., & LIOY, P.J. 2000. Seasonal influences on childhood lead exposure. *Environmental Health Perspectives*, **108**, 177-182.

Using Ground Penetrating Radar to delineate sub-surface calcrete in the Great Victoria Desert, South Australia: implications for gold exploration

Melvyn J. Lintern[1], Anton W. Kepic[2] & Matthew Josh[3]
[1]*CSIRO Exploration & Mining, P.O. Box 1130, Bentley, 6102 WESTERN AUSTRALIA (e-mail: mel.lintern@csiro.au)*
[2]*Head of Department, Exploration Geophysics, Curtin University, 26 Dick Perry Avenue, Kensington, 6151 WESTERN AUSTRALIA.*
[3]*CSIRO Petroleum Resources, P.O. Box 1130, Bentley, 6102 WESTERN AUSTRALIA*

ABSTRACT: Exploration in southern Australia is commonly hampered by the presence of exotic cover such as aeolian sand and alluvium. Calcrete (caliche), present within the cover, has been shown to assist mineral explorers searching for Au deposits as it is an easily identifiable material that can accumulate Au. However, in large areas of South Australia, the location of calcrete within the cover is hampered by overlying sand. Here, we use ground penetrating radar to expose the location of calcrete at the Edoldeh Tank Au deposit, suggest how calcrete can form in the sub-surface, and demonstrate how Au in calcrete can extend the surficial geochemical footprint of Au deposits and thus provide a broader target for explorers.

KEYWORDS: *calcrete, gold exploration, ground penetrating radar, mineral exploration, calcium carbonate*

INTRODUCTION

Calcrete (caliche) or pedogenic carbonate sampling is an important technique for gold exploration, particularly in Australia. In South Australia, mineral explorers use augers or manually dig holes and collect calcrete from the near surface. Typically, calcrete accumulates in arid/semi-arid conditions in South Australia as a result of wind blown dust, rainfall and aerosol derived from marine sources. As calcrete forms sub-surface its appearance in undisturbed environments is commonly disguised by soil and other regolith materials. Calcrete may be ubiquitous in some areas but in sand dune environments its precise distribution in the landscape is not well known. Augering or digging for calcrete here is a hit and miss procedure and add significantly to exploration expenditure. Therefore, an appreciation of calcrete distribution in the landscape is important to mineral exploration.

METHOD AND RESULTS

The distribution and possible processes of formation of calcrete was investigated at Edoldeh Tank Au prospect in the western Gawler Craton, located on the edge of the Great Victoria Desert (GVD). In this part of the GVD, regolith landforms are comprised of scarce hills of weathered bedrock outcrops surrounded by sand spreads, dunes and colluvial materials; the hills act as windows to the otherwise covered weathered bedrock. The outcrops themselves have been silicified and, more recently, have been overprinted with calcrete. Calcrete sampling is relatively easy on the exposed outcrops and is preferentially sampled by mineral explorers due to its near-surface location (<10-20 cm depth). However, calcrete on the colluvial slopes and in the swales is not as easily located because of concealment by GVD sand and colluvium.

Ground Penetrating Radar (GPR) was selected to be the primary technique for mapping the calcrete extent because it has very good resolution (less than 0.3 m for a 250 MHz system) and in dry sand/rock can map geological features down to about 10 m (at 250 MHz) depth before attenuation and scattering reduce the signal. Other geophysical techniques generally lack sufficient contrast or resolution to be useful. Seismic methods

can detect consolidated layers very well and have reasonable resolution at shallow depths, but are at least an order of magnitude slower in this environment and cannot detect the base of the calcrete easily. Data were collected for 250 and 500 MHz antenna, and spatial sampling was set by constant time interval and a slow, but steady rate of progress with markers set in the data for 20 m tape intervals. A stack of 32-64 pulses were recorded every 5 cm or less. A surprise in the GPR data was its lack of penetrating power through the cover. The GPR data required more than usual gain adjustment and signal processing to preserve the amplitude variations of reflectivity that mark the calcrete boundaries. As the signal was often at the level of residual systematic noise a long interval 2D subtraction filter was used to extract the reflectivity variations. Whilst the calcrete itself seems fairly transparent, although irregular, it appears that the very dry quartz sand (>90% silica) highly attenuates GPR signals; possibly due to a thin coating of iron rich clay over each silica particle. Surveys upon a nearby track over small sand dunes appear to confirm this characteristic.

Five E-W and N-S transects were selected for the GPR survey. These were located below the flanks of a low hill strewn with silcrete and silicified weathered bedrock cobbles and gravels. Previous limited drilling indicated that the thickness of exotic sandy cover was about 5 m and that calcareous materials may be patchily distributed.

The GPR survey data showed a consistent zone of resistance located at ~0.5-1 m below the surface for each of the five E-W transects. Stacking the graphical images of the transect data, according to their locations on the plan, reveals a tongue-shaped structure of resistance that extends southwards (down slope) at least 200 m visible on all five transects. The depth of resistance is consistent with a sub surface enrichment of calcrete.

In order to test this hypothesis, 25 shallow pits were dug along the transect lines through the sand in areas of high and low resistance. The zones of high resistance were coincident with the appearance of a near-surface hard laminated calcareous hardpan while the zones of low resistance either had poorly-developed calcareous materials, powdery pedogenic carbonate and/or nodular calcrete.

The often smooth top surface to the calcrete suggests that the calcrete formed by the precipitation of Ca (as carbonate) from sub-surface laterally and vertically flowing vadose water sourced from rainfall, which penetrates easily through the overlying sand. The sub-surface has been plugged with calcrete preventing vertical downwards penetration of vadose water. Instead, vadose water would move laterally until it evaporates or is removed by transpiration. Precipitation of calcium carbonate at the surface of the calcrete would occur, thus contributing to the laminated occurrence of the calcrete.

DISCUSSION

The tongue-shaped calcrete structure delineated by the GPR has likely to have been formed in one of two ways: either it is the remnant of a more widespread calcrete platform that once covered the entire study area as a result of horizontal movement of fluids and detritus downslope of the hill or it signifies a palaeochannel formed as a result of vadose water preferentially flowing and precipitating in confined zone. The current topography shows a gradient from the NW to the SE within which ephemeral drainages have developed. There is an absence of laminar calcrete accumulation in the near surface of the ephemeral drainages. Deep trenching through the calcrete and sedimentological analysis is required to further investigate these possible explanations of the calcrete tongue formation. Either way, Ca has been transported downslope.

The significance of the calcrete tongue became apparent after geochemical analysis of samples from the test pits showed elevated Au concentrations. Importantly, the highest concentrations (>50 ppb Au) were confined to the laminar

calcrete of the tongue. The source of the Au is from the hill where elevated Au concentrations have been found in the weathered basement. The Au in calcrete down slope of the hill represents a significant extension to the surficial geochemical anomaly and provides a broader target for exploration both at Edoldeh Tank and for similar landscape settings in the GVD. It suggests that Au anomalies in calcrete can be transported but still retain their anomalous signature and thus provide a vector to mineralisation.

CONCLUSIONS

Ground Penetrating Radar was successfully used to delineate an otherwise undetectable sub-surface calcrete structure. The origin of the structure is a result of surficial processes related to rainfall and topography. Elevated Au concentrations in the calcrete provide a broader target for exploration and suggest that "transported" chemically-mobilised pedogenic carbonate can retain a geochemical signature developed above upslope mineralisation sources.

ACKNOWLEDGEMENTS

We thank David Gray and Nathan Reid for commenting on earlier versions of the manuscript.

A new direction in searching for the atmospheric CO_2 sink: considering the joint action of carbonate dissolution, global water cycle and the photosynthetic uptake of dic by aquatic organisms

Zaihua Liu[1,2,*], Wolfgang Dreybrodt[3], & Haijing Wang[4]

[1] *The State Key Laboratory of Environmental Geochemistry, Institute of Geochemistry, Chinese Academy of Sciences, Guiyang 550002 CHINA (e-mail: liuzaihua@vip.gyig.ac.cn)*

[2] *Karst Dynamics Laboratory, Institute of Karst Geology, Guilin 541004 CHINA*

[3] *Institute of Experimental Physics, University of Bremen, Bremen 28334 GERMANY*

[4] *School of Geographical Sciences, Southwest University, Chongqing 400715 CHINA*

ABSTRACT: The locations, magnitudes, variations and mechanisms responsible for the atmospheric CO_2 sink are uncertain and under debate. Previous studies concentrated mainly on oceans, and soil and terrestrial vegetation as sinks. Here, we show that there is an important CO_2 sink in carbonate dissolution, the global water cycle and photosynthetic uptake of DIC by aquatic ecosystems. The sink constitutes up to 0.82 Pg C/a: 0.24 Pg C/a is delivered to oceans via rivers and 0.22 Pg C/a by meteoric precipitation, 0.12 Pg C/a is returned to the atmosphere, and 0.23 Pg C/a is stored in the continental aquatic ecosystem. The net sink could be as much as 0.70 Pg C/a, may increase with intensification of the global water cycle, increase in CO_2 and carbonate dust in atmosphere, reforestation/afforestation, and with fertilization of aquatic ecosystems. Under the projection of global warming for the year 2100, it is estimated that this CO_2 sink may increase by 22%, or about 0.18 Pg c/a.

KEYWORDS: *atmospheric CO_2 sink, carbonate dissolution, global water cycle, aquatic photosynthesis, organic matter storage/burial*

INTRODUCTION

An important problem in the science of global change is the imbalance of the atmospheric CO_2 budget (Melnikov & O'Neill, 2006). Of the CO_2 added to the atmosphere from burning of fossil fuels, ~half stays in the atmosphere and ~half is absorbed into the oceans and terrestrial biosphere. Some is "missing". Without correct accounting, predictions resulting from CO_2 emission scenarios are uncertain and the uncertainty affects energy policy decisions.

Previous studies addressed oceans and terrestrial vegetation as CO_2 sinks. Here, we describe an important CO_2 sink in carbonate dissolution, the global water cycle (GWC), and uptake of dissolved inorganic carbon (DIC) by aquatic. The sink is larger than previous estimates (Meybeck 1993; Gombert 2002).

METHODS

The CO_2 hydrologic sink (J_T) is:

$$J_T = Q_{MP} \times C_{DIC,MP} + Q_{RO} \times C_{DIC,RO} \quad (1)$$

where Q_{MP} is meteoric precipitation and Q_{RO} is continental runoff (Shiklomanov 1993), $C_{DIC,MP}$ is the mean observed meteoric precipitation DIC concentration, and $C_{DIC,RO}$ is the calculated DIC in equilibrium with world mean soil CO_2 and/or calcite.

$C_{MP,DIC}$ was based on MP falling on oceans. $C_{DIC,RO}$ is computed, using the DIC of soil pore water in equilibrium with a soil air pCO_2 and/or calcite (Dreybrodt 1988). Global mean soil pCO_2 was calculated as (Brook *et al*. 1983):

$$\log(pCO_2) = -3.47 + 2.09(1 - e^{-0.00172\,AET}) \quad (2)$$

where AET is annual evapotranspiration, and weighted for carbonate (~15% of the land area; Ford & Williams 1989; Gombert 2002) and non-carbonate regions.

The net CO_2 sink for RO ($J_{N,RO}$) is:

$$J_{N,RO} = J_{TC} - J_{DG,RO} \quad (3)$$

where J_{TC} is CO_2 sink by the dissolution of carbonate and CO_2, and $J_{DG,RO}$ is CO_2 degassed from RO waters (Einsele *et al*. 2001; Lerman & Mackenzie 2005).

CALCULATION OF GWC CO_2 SINKS

Figure 1 presents the model. Precipitation rates are: 9000 km^3 between atmosphere and continental interior (CI), 110000 km^3 between atmosphere and continental margins (CM), and 458000 km^3 between atmosphere and oceans. Mean DIC for global precipitation is 81.59 μmol/l. Thus, the atmospheric CO_2 sink is 0.0044, 0.054, and 0.22 Pg C/a, respectively (Fig. 1). Annual global CI RO and CM RO are 2000 and 44800 km^3, respectively (Baumgartner & Reichel 1975; Shiklomanov 1993). Using global mean soil pCO_2 of 6393 ppmv and global mean surface temperature of 15°C, the equilibrium values of DIC are 300 and 3640 μmol/l for the non-carbonate and carbonate terranes, respectively. Thus, CO_2 sinks by CI and CM RO are 0.013 and 0.28 Pg C/a, respectively.

The total calculated CO_2 sink of 0.30 Pg C/a is very close to that of Gombert (2002; 0.302 Pg C/a), who used a different approach. Although our method seems valid, in terranes with large amounts of pedogenic carbonate (48% continental area; Adams & Post 1999), the continental-RO CO_2 sink will be larger. Using 50% of land area as a conservative estimate of karst regions and soil with pedogenic carbonate, CO_2 sinks by CI and CM RO are estimated to be 0.025 and 0.57 Pg C/a, respectively (Fig. 1). Therefore, the total atmospheric CO_2 sink as DIC by the GWC could be 0.82 Pg C/a.

DIC is removed during photosynthesis (the "biological pump"; Maier-Reimer 1993) or returned to the atmosphere. Lerman and Mackenzie (2005) found that net storage of organic carbon counteracts CO_2 production by carbonate precipitation: $Ca^{2+} + 2HCO_3^- \Leftrightarrow CaCO_3 + CH_2O + O_2$. Iglesias-Rodriguez *et al*. (2008) studied phytoplankton calcification in a high-CO_2 world, finding that calcification and net primary production in the coccolithophore *Emiliania huxleyi* are increased by high CO_2 partial pressures: over the past 220 years there has been a 40% increase in average coccolith mass.

River- and lake-surface areas are small compared with those of land and ocean, and so direct exchange of carbon

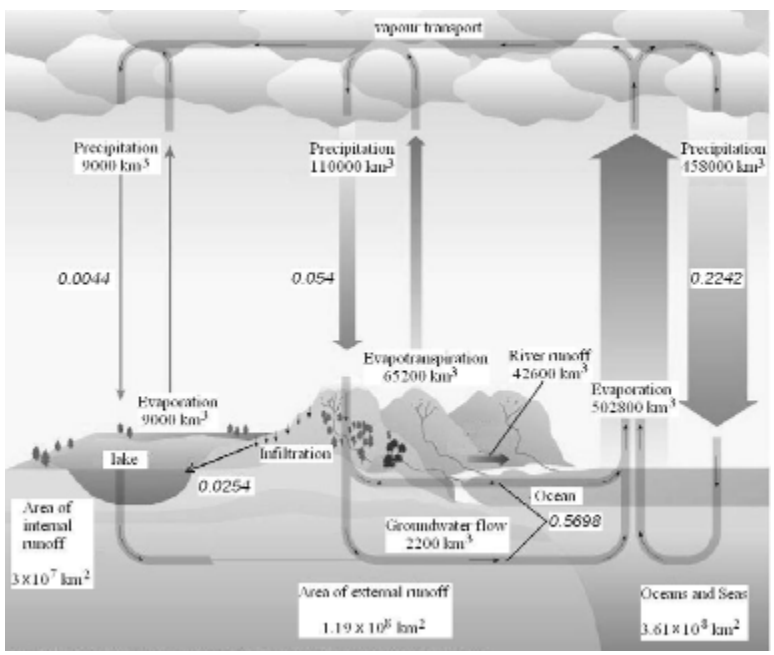

Fig. 1. The global water cycle and its CO_2 sinks (italic numbers, in Pg C/a; water fluxes from Shiklomanov 1993).

between rivers/lakes and atmosphere is possibly less important (Kling *et al*. 1991). However, the rivers of the world are conduits between the land and ocean or inland lakes, carrying large amounts of carbon to the ocean or inland lakes (Kempe 1984; Meybeck 1993).

If 0.24 Pg C/a represents riverine DIC delivered to oceans (Meybeck 1993) and if the flux of carbon from rivers/lakes to the atmosphere is 20% (Kling *et al*. 1991) of the total (i.e., 0.12 Pg C/a), then 0.23 Pg C/a remains in inland lakes and rivers, and in slowly cycled groundwater. Cole *et al*. (2007) estimated that about 0.2 Pg C/a is buried in inland water sediments. Groundwater may have a greater carbon storage capacity due to its large volume and greater load of carbon than rivers (Kempe 1984).

Carbon flux from the oceans to atmosphere can be neglected, because oceans are a large net atmospheric CO_2 sink (Sabine *et al*. 2004).

FUTURE OF THE GWC SINK

The GWC sink for CO_2 may increase with intensification of the hydrologic cycle (Huntington 2006), including increase in MP DIC (increase in atmosphere pCO_2 and carbonate dust) and in RO DIC (due to reforestation; Liu & Zhao 2000).

Climate-warming enhanced RO could be 2~5% per degree (Huntington 2006). Climate models predict average global surface temperature rise of 1.1 to 6.4 °C during the 21st century. Using a temperature increase of 3.75°C and precipitation increase of 13%, the GWC CO_2 sink may increase by 13% if the DIC of MP and RO are unchanged. For an increase in atmosphere pCO_2 from 350 ppmv to 700 ppmv, MP DIC is estimated to increase by 21% ($CaCO_3$-CO_2-H_2O system) to 83% (CO_2-H_2O system). Increases in AET and reforestation/ afforestation may cause soil CO_2 to increase (Liu & Zhao 2000). Assuming AET also increases 13%, world mean soil pCO_2 will increase from 6393 ppmv to 7936 ppmv (formula by Brook *et al*. 1983; ~24% increase), a conservative estimate in that it ignores potential soil CO_2 increase by fertilization and reforestation. Macpherson *et al*. (2008) determined that groundwater pCO_2 in Konza Prairie, USA increased by about 29% (2100ppmv) from 1991-2005. RO DIC is thus estimated to increase by 3.57%. Taking all these into account, the GWC CO_2 sink may increase by ~22% (~0.18 Pg c/a) by the year 2100. Raymond *et al*. (2008) found that the bicarbonate flux from the Mississippi River increased from 0.01 Pg c/a to 0.015 Pg c/a (46% increase) during the past 50 years. This change was attributed mostly to land-use changes rather than climate change.

CONCLUSIONS AND PERSPECTIVE

We have shown an important potential CO_2 sink by joint action of carbonate dissolution, GWC and the photosynthetic uptake of DIC by aquatic. The sink constitutes up to 0.82 Pg C/a: 0.47 Pg C/a goes to sea via continental rivers and precipitation over sea, 0.12 Pg C/a is returned to the atmosphere, and 0.23 Pg C/a is stored in the continental aquatic ecosystem. The net sink, then, could be 0.70 Pg C/a, or ~9% of the total anthropogenic CO_2 emission and 25% of the missing CO_2 sink (Melnikov & O'Neill 2006).

This sink, a negative climate feedback mechanism, may increase with the global-warming-intensified GWC, the increase in CO_2 and carbonate dust in atmosphere, reforestation/afforestation, and fertilization of the aquatic ecosystems. Using the global warming projection for the year 2100 by IPCC, it is estimated that the CO_2 sink by the GWC will increase by ~22%, or ~0.18 Pg c/a.

Important, poorly-constrained variables in this carbon balance include temporal and spatial variations in precipitation and RO DIC, carbonate dust, and pedogenic carbonate and soil CO_2. In addition, ocean and lake response to river carbon input is not well known. Although marine and freshwater aquatic organisms can be fertilized by increases in N, P, Si, Fe, Zn and CO_2 (Cassar *et al*. 2004; Zondervan 2007), it is not clear how much of the

carbon is trapped in lakes, estuaries and coastal zones, and how much is returned to the atmosphere through respiration (Zondervan 2007).

This paper presents an estimate of the CO_2 sink by carbonate dissolution, GWC and photosynthetic uptake of DIC by aquatic ecosystems, and suggests a new direction in balancing the global C budget.

ACKNOWLEDGEMENTS

This work was supported by the Hundred Talents Program of Chinese Academy of Sciences, and National Natural Science Foundation of China (Grant No. 40872168).

REFERENCES

ADAMS, J.M. & POST, W.M. 1999. A preliminary estimate of changing calcrete carbon storage on land since the Last Glacial Maximum. *Global and Planetary Change*, **20**, 243–256.

BAUMGARTNER, A. & REICHEL, E. 1975. *The World Water Balance.* Elsevier, Amsterdam.

BROOK, G.A., FOLKOFF, M.E., & BOX, E.O. 1983. A world model of soil carbon dioxide. *Earth Surface Processes and Landforms,* **8**, 79-88.

CASSAR, N., LAWS, E.A., BIDIGARE, R.R., & POPP, B.N. 2004. Bicarbonate uptake by Southern Ocean phytoplankton. *Global Biogeochemical Cycles,* **18**, doi: 10.1029/2003GB002116.

COLE, J.J. & PRAIRIE, Y.T. *et al*. 2007. Plumbing the global carbon cycle: Integrating inland waters into the terrestrial carbon budget. *Ecosystems*, **10**, 171–184.

DREYBRODT, W. 1988. *Processes in karst systems.* Springer, Heidelberg.

EINSELE, G., YAN, J., & HINDERER, M. 2001. Atmospheric carbon burial in modern lake basins and its significance for the global carbon budget. *Global and Planetary Change*, **30**, 167–195.

FORD, D.C. & WILLIAMS, P.W. 1989. *Karst Geomorphology and Hydrology.* Unwin Hyman, London.

GOMBERT, P. 2002. Role of karstic dissolution in global carbon cycle. *Global and Planetary Change***, 33**, 177-184.

HUNTINGTON, T. G. 2006. Evidence for intensification of the global water cycle: Review and synthesis. *Journal of Hydrology*, **319**, 83-95.

IGLESIAS-RODRIGUEZ, M.D. & HALLORAN, P.R. *et al*. 2008. Phytoplankton calcification in a high-CO_2 world. *Science,* **320**, 336-340.

KEMPE, S. 1984. Sinks of anthropogenically enhanced carbon cycle in surface fresh waters. *Journal of Geophysical Research*, **89**, 4657–4676.

KLING, G.W., KIPPHUT, G. W. & MILLER, M.C. 1991. Arctic lakes and streams as gas conduits to the atmosphere: Implications for tundra carbon budgets. *Science*, **251**, 298-301.

LERMAN, A. & MACKENZIE, F.T. 2005. CO_2 air-sea exchange due to calcium carbonate and organic matter storage, and its implications for the global carbon cycle. *Aquatic Geochemistry,* **11**, 345-390.

LIU, Z. & ZHAO, J. 2000. Contribution of carbonate rock weathering to the atmospheric CO_2 sink. *Environmental Geology*, **39**, 1053-1058.

MACPHERSON, G.L. & ROBERTS, J.A. *et al*. 2008. Increasing shallow groundwater CO_2 and limestone weathering, Konza Prairie, USA. *Geochimica et Cosmochimica Acta*, **72**, 5581-5599.

MAIER-REIMER, E. 1993. The biological pump in the greenhouse. *Global Planet Change*. **8**, 13-15.

MELNIKOV, N.B. & O'NEILL, B.C., 2006. Learning about the carbon cycle from global budget data. *Geophysical Resear Letters,* **33**, doi:10.1029/ 2005GL023935.

MEYBECK, M. 1993. Riverine transport of atmospheric carbon: sources, global typology and budget. *Water, Air, and Soil Pollution,* **70**, 443-463.

RAYMOND, P.A. & OH, N.H. *et al*. 2008. Anthropogenically enhanced fluxes of water and carbon from the Mississippi River. *Nature*, **451**, 449-452.

SABINE, C.L. & FEELY, R.A. *et al*. 2004. The oceanic sink for anthropogenic CO_2. *Science*, **305**, 367-371.

SHIKLOMANOV, I.A. 1993. World fresh water resources. In: Gleick, P.H. (ed) *Water in Crisis: A Guide to the World's Freshwater Resources*. Oxford University Press, New York, USA, 13-24.

ZONDERVAN, I. 2007. The effects of light, macronutrients, trace metals and CO_2 on the production of calcium carbonate and organic carbon in coccolithophores—A review. *Deep-Sea Research II*, **54**, 521–537.

Groundwater CO_2: is it responding to atmospheric CO_2?

G. L. Macpherson
Department of Geology, University of Kansas, 1475 Jayhawk Blvd., Lawrence, KS 66044, USA
(e-mail: glmac@ku.edu)

ABSTRACT: Carbon dioxide in groundwater is typically 10-100 times higher concentration than the atmosphere. In a shallow, thin limestone aquifer in the central USA, dissolved CO_2 varies seasonally, lagging the atmosphere's CO_2 cycle by about 6 months. Besides the annual cycle, dissolved CO_2 has increased at this tallgrass prairie research site during the monitoring period of the past 20 years. Although the precise mechanism is unknown, the similarities in the annual trends of atmospheric CO_2 and groundwater CO_2 at this site suggest there is a tight link between the two CO_2 reservoirs. These similarities include the peak width at CO_2 minima, peak width at CO_2 maxima, and the 20-year trend of overall increase. Groundwater CO_2 at this site has been increasing at a rate that is ~100 times greater than the increase in atmospheric CO_2, suggesting that groundwater may be a significant and active sink for CO_2. The most probable source for the shallow groundwater CO_2 at this site is soil respiration; soil respiration must be responding to climate change or atmospheric CO_2, thus creating the similar trends in atmospheric and groundwater CO_2.

KEYWORDS: *CO_2, groundwater, climate change, sequestration, soil respiration*

INTRODUCTION

The global C budget is acknowledged to have a large impact on Earth's climate (IPCC 2007), and yet, as we currently understand it, there is a large mismatch between C sources and sinks, with at least 1 Pg C yr^{-1} having no apparent sink. Until recently (e.g., Cole et al. 2007; Liu et al. 2008), the involvement of the terrestrial water cycle in the global C budget had been largely ignored.

Estimates of CO_2 sequestration in groundwater, both from incorporation of soil CO_2 and transformation to dissolved inorganic carbon (DIC), vary over an order of magnitude. Kessler and Harvey (2001) estimate the global flux of C to groundwater to be 0.02 Pg C yr^{-1}. This estimate is based on only 44 CO_2 measurements that are biased to western North America. Andrews and Schlesinger (2001), based on data from the Duke Forest Free Air CO_2 Enrichment (FACE) experiments, estimate that under ~1.5X present CO_2, the global C flux to groundwater would increase to 0.12 Pg C yr^{-1}. The estimate for increased C flux to groundwater by Andrews and Schlesinger (2001) is nearly equal to the estimate of Liu et al. (2008) for the current global flux of 0.13 Pg C yr^{-1} to the continental aquatic ecosystem. In effect, based on the above estimates, the flux of C to groundwater could account for ~2% to ~12% of the missing carbon sink in the global carbon budget.

The recent finding (Macpherson et al. 2008) that groundwater CO_2 is increasing ~100 times faster than atmospheric CO_2 draws attention to our limited understanding of the link between the atmosphere and shallow groundwater in terms of gas transfer and storage. This abstract investigates this link and presents evidence for a tight coupling between atmospheric and groundwater CO_2.

SETTING

The study area is the bottom fourth of a 1.2 km^2 upland watershed within the 35 km^2 Konza Prairie (fig. 1). The Konza Prairie is located within the Flint Hills physiographic province, which is an unplowed, ~50,000 km^2 remnant of original tallgrass prairie; 99% of the original prairie has been plowed. The study area climate is temperate mid-continental. Annual meteoric precipitation

is 835±190 mm and 75% of precipitation falls during the growing season (Knapp et al. 1998).

Bedrock at the Konza Prairie is Permian-aged, alternating, thin (1-3 m) limestones and thicker (2-12 m) shales. Soils are mostly less than 1 m thick, and form on bedrock, Pleistocene-aged loess, and alluvium and colluvium.

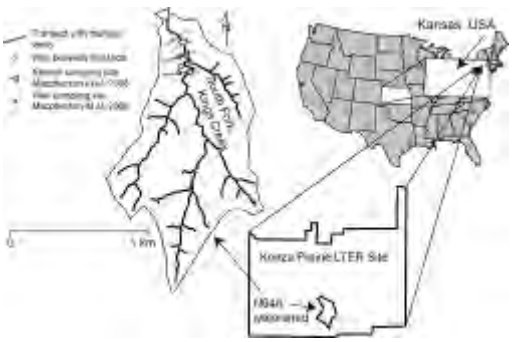

Fig. 1. Study area is the Konza Prairie Long-Term Ecological Research Site and Biological Station, a native tallgrass prairie.

HYDROGEOCHEMISTRY

The essentially unconfined limestone aquifers at the Konza Prairie respond rapidly to precipitation and supply base flow to, and are recharged by, the stream draining the watershed (Macpherson 1996). One aquifer, the subject of this paper, has been sampled almost every 4-6 weeks since 1991. The ~5 cm diameter PVC well used in this abstract is ~12 m deep and is screened only in the limestone. Other wells at the site have similar chemistry to the well used here. (Details about sampling and analysis protocols can be found in Macpherson et al., 2008.) Increasing alkalinity (fig. 2), alkaline earth cations, and groundwater CO_2 suggest increasing weathering of carbonate minerals (Macpherson et al. 2008), a significant portion of which may be allochthonous carbonate dust that has more radiogenic Sr than the bedrock (Wood & Macpherson 2005).

CARBON DIOXIDE

The annual cycle of higher and lower

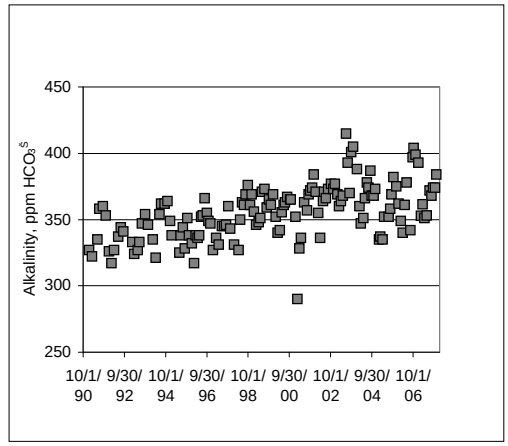

Fig. 2. Increase in titration alkalinity of groundwater from a thin limestone aquifer iin the central USA over the study period is accompanied by increasing groundwater CO_2 and decreasing pH (not shown).

groundwater CO_2 (Macpherson et al., 2008) mimics the Niwot Ridge, Colorado, atmospheric CO_2 annual cycle (Tans & Conway 2005), the atmosphere monitoring station closest to the study area. The groundwater cycle lags the atmosphere cycle by ~six months (fig. 3). Groundwater CO_2 is ~10 to 100 times higher concentration than atmosphere CO_2, so a direct transfer of CO_2 from the atmosphere to groundwater is unlikely.

The patterns in the atmosphere CO_2 cycle, with longer duration of CO_2 maxima and shorter duration of CO_2 minima, are repeated in the groundwater CO_2 cycle (fig. 3). In addition, when the atmosphere cycle has a longer CO_2 minimum (e.g., August-September, 1998, on fig. 3) then the groundwater cycle has a longer CO_2 minimum (e.g., February-April, 1999, on fig. 3). Similarly, when the atmosphere has a short period of minimum CO_2, (e.g., August, 1999, on fig. 3), the lagged groundwater signal also has a short period of minimum CO_2 (e.g., March, 2000, on fig. 3). Similarities in curve shape also occur at times of CO_2 maxima.

DISCUSSION

The higher partial pressures of CO_2 in the groundwater preclude simple transport

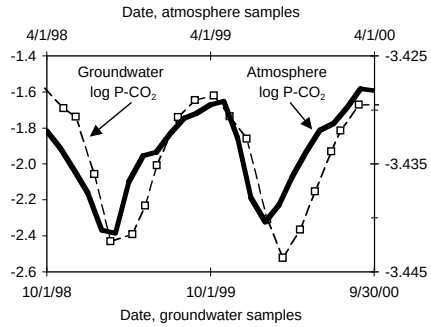

Fig. 3. Example of similarity between atmospheric CO_2 and groundwater CO_2 annual cycles. The groundwater cycle lags the atmosphere cycle by ~ 6 months.

of lower partial pressure CO_2 from the atmosphere to the higher partial pressure CO_2 in the aquifer. Stable carbon isotope data (unpublished) suggest that respiration-derived CO_2 dissolving marine limestone is one reasonable explanation for the source of CO_2. Although aboveground net primary productivity (ANPP) does not show a trend over the time period of this study (Macpherson et al. 2008), ANPP has a large standard deviation, in that it responds primarily to moisture. Meteoric precipitation in this region is highly variable (annual variability ~20-25%; monthly variability > 100%; Macpherson, 1996), and so ANPP correlates strongly with annual precipitation. The ANPP data set is not long enough to show a long-term trend on top the annual variability.

Belowground biomass is greater than aboveground biomass in grasslands, and yet the BNPP is difficult to quantify, so it is unknown whether belowground biomass has changed at the site. In addition, if microbial activity is stimulated by higher ambient CO_2, as it is in experiments (Williams et al. 2000), and if microbes breakdown recent organic matter more rapidly than old organic matter (Cardon et al. 2001), then ANPP or BNPP might not change even as total primary productivity and respiration increase. This scenario increases respiration-derived CO_2 that might be delivered to the groundwater as well as to the atmosphere.

CONCLUSIONS

Groundwater CO_2 at the Konza Prairie LTER Site, an unplowed, mid-continental, mesic tallgrass prairie used for ecological research, has increased over the past 20 years, along with alkalinity and alkaline earth cations. The change in groundwater CO_2 over the study period has been about 100 times larger than the change in atmospheric CO_2 concentration over the same period. The annual groundwater CO_2 cycle has a pattern similar to the annual pattern of CO_2 in the atmosphere, with longer periods of high CO_2 than low CO_2 in any year, as well as similar durations of low-CO_2 periods, the length of which change from year to year. A direct transfer of CO_2 from the atmosphere to groundwater is unreasonable, because groundwater CO_2 concentrations are always 10 to 100 times higher than atmospheric concentrations. An increase in soil respiration, with or without increases in ANPP or BNPP, is proposed as a more reasonable explanation for the increasing groundwater CO_2. The increase in groundwater CO_2 strongly suggests that shallow groundwater is a significant sink for CO_2.

ACKNOWLEDGEMENTS

I thank the Konza Prairie LTER for funding through the NSF LTER Program, the Dept. of Geology at the University of Kansas, and the Geology Endowment Fund of the University of Kansas for supplementary funding. I also am grateful to Marios Sophocleous for providing Palmer Drought Index data for the region, and to the numerous students over the years who helped with data collection for this project.

REFERENCES

CARDON, *et al.* 2001. Contrasting the effects of elevated CO2 on old and new soil carbon pools. *Soil Biology and Biochemistry*, **33**, 365-373.

COLE, J.J. *et al.* 2007. Plumbing the global carbon cycle: Integrating inland waters into

the terrestrial carbon budget. *Ecosystems,* **10,** 171-184. DOI: 10.1007/s10021-006 9013-8.

INTERGOVERNMENTAL PANEL ON CLIMATE CHANGE (IPCC). 2007. *Climate change, 2007, the fourth IPCC assessment report*. IPCC.

KESSLER, T.J. & HARVEY, C. S. 2001. Global flux of CO_2 into groundwater. *Geophysical Research Letters*, **28**, 279-282.

KNAPP, A.K. et al., eds. 1998. *Grassland Dynamics*. Oxford University Press, New York.

LIU, Z., *et al.* 2008. A possible important CO_2 sink by the global water cycle. *Chinese Science Bulletin*, **53,** 402-407.

MACPHERSON, G.L. ET AL. 2008. Increasing shallow groundwater CO_2 and limestone weathering. *Geochimica et Cosmochimica Acta,* **72**, 5581-5599. doi:10.1016/j.gca. 2008.09.004

MACPHERSON, G.L., 1996. Hydrogeology of thin limestones—the Konza Prairie LTER Site. *Journal of Hydrology*, **186**, 191-228.

TANS P.P. & CONWAY T.J. 2005. Monthly atmospheric CO_2 mixing rations from the NOAA CMDL Carbon Cycle Cooperative Global Air Sampling Network, 1968-2002. In *Trends: A Compendium of Data on Global Change, Carbon Dioxide Information Center*. Oak Ridge National Laboratory, U.S. Dept. of Energy, Oak Ridge, Tenn., USA.

WILLIAMS M. A. *et al.* 2000. Carbon dynamics and microbial activity in tallgrass prairie exposed to elevated CO_2 for 8 years. Plant and Soil, **227**, 127-137.

WOOD, H. K. & MACPHERSON, G.L. 2005. Sources of Sr and implications for weathering of limestone under tallgrass prairie, northeastern Kansas. *Applied Geochemistry,* **12**, 2325-2342; doi:10.1016/ j.apgeochem.2005.08.002.

Lithological Identification of Rocks in Cape Smith Fold Belt Region; New Quebec Using Remote Sensing Applications

Yask N. Shelat[1] & James E. Mungall[1]
[1]*Department of Geology, University of Toronto, Earth Science Centre; 22 Russell Street, Toronto ON M5S 3B1*
(e-mail: yask.shelat@gmail.com)

ABSTRACT: A study was performed to validate use of remote sensing data for the identification of rock units at Cape Smith fold belt region, New Quebec, Canada. Remote sensing advancement has facilitated to characterise the properties of rock units over a large area with a lot less time than traditional field work. The study area is mainly composed of peridotite, gabbro, metabasalt, metasediments etc and mapped previously by the second author. Landsat Enhanced Thematic Mapper (ETM+) imagery (30 m spatial resolution; bands 1 to 5 and 7) was used to perform various remote sensing techniques such as Band Ratio, Principal Component Analysis, and Supervised Classification. The Remote Sensing image results showed good agreement with the available geological map.

KEYWORDS: *Remote Sensing Geology, Landsat Enhanced Thematic Mapper, Band Ratio, Principal Component Analysis, Supervised Classification*

INTRODUCTION

Remote sensing technology is now becoming an increasingly important means for resource exploration. Use of satellite imagery, image processing, and the correlation of processed images with geological map have been emerging as an effective tool for creating and refining geological map with further structural and lithologic information. (Krishnamurthy 1997; Sabins 1999; Gad *et al.* 2005; Khan *et al.* 2006).

A study was performed to identify rock units in the Cape Smith fold belt, New Quebec orogen, using remote sensing techniques. This region was studied and mapped (Mungall 2007). Enhanced Thematic Mapper (ETM+) image, having 30 m spatial resolution with 8 bit data format, (acquired during the year 2000, Path/Row-20/17 at UTM N 61.48/ W 074.42) was used in this study. The orthorectified satellite imagery of concerned area was supplied by Canadian Royalties Inc. The Landsat data was processed by several different image enhancement techniques, such as Band Ratio analysis and Principal Component Analysis. Supervised Classification was also applied for the same purpose on resultant RGB image (5,4,2) obtained from PCA analysis (Krishnamurthy 1997; Sabins 1999; Gad *et al.* 2005; Lillesand *et al. 2007*)

GEOLOGICAL SETTING

The geology description of Cape Smith fold belt is separated into two domains, namely the northern allochthonous and southern parautochthonous (see Mungall 2007). These domains were highly affected by the Trans-Hudson orogeny (~1830-1840 Ma). The southern part of the domain contains Povungnituk and Chukotat groups. The geological map and stratigraphy of the area is presented in Figure 1.

The Dumas Formation is uncomformably overlying the Archean Superior Province. It hosts metasediments and intercalated iron formations, as well as peridotite and gabbro bodies, which were identified and separated with the help of both Band ratio and Principal Component Analysis.

The Beauparlant Formation is produced during major volcanic activity that occurred between 2038 and 1991 Ma. It consists of upper, middle, and lower members composed of sheet and pillowed

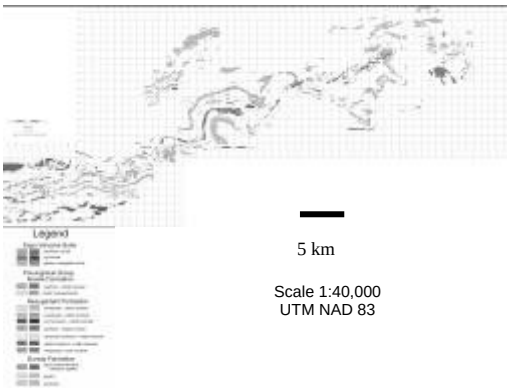

Fig. 1. Geological Map of the Cap smith fold belt and Expo Intrusive Suite (see Mungall 2007).

basalts with metasedimentary intercalations. Magnetic highs occur in the middle member of the formation.

The Expo Intrusive Suite is for the most part composed of mafic and ultramafic intrusions, shaped as tabular-shaped discordant bodies, so are referred as dykes. The Expo suite is economically important due to the presence of sulfide mineralization in the internal part of the intrusion. It is composed of gabbro norite, pyroxenite, peridotite, and dunite.

METHODS & RESULTS

The flow diagram (Fig. 2) outlines the methods used for the review and separation of the rocks present in the area. Image enhancement is done to increase the variance in the dataset. Contrast manipulation, spatial feature manipulation, and multi-image manipulation are used as digital enhancement techniques (Lillesand *et al. 2007*). In this study multi-image manipulation is used, which includes Band Ratio and Principal Component Analysis.

Band Ratio

The Band ratio approach for the lithology identification was taken previously by many authors (Sabins 1999; Gad *et al*. 2005; Khan *et al*. 2006).

The Band Ratio enhancement technique can be used to remove the brightness variation caused by topographic effects in a region. (Gad *et al*. 2005; NASA Remote sensing tutorial by Dr. Nicholas Short)

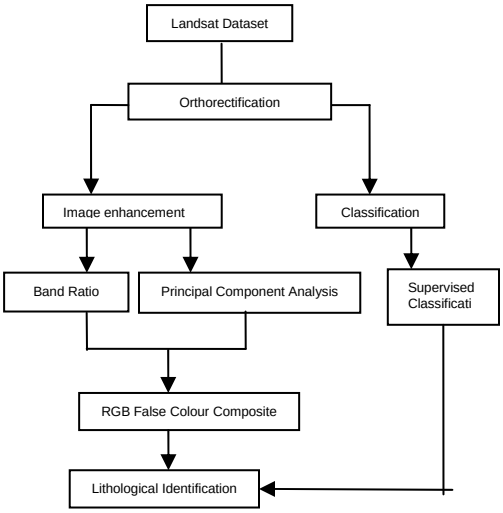

Fig. 2. Flow Chart showing the methods used for the identification of the rocks.

Two objects with different spectral properties, i.e., variation in the slope of spectral reflectance curve of two bands, can be separable with the help of ratio images (Lillesand *et al. 2007*). In this study standard reflectance data of USGS Spectral Library and John Hopkins University spectral library (Available in ENVI) have been used. To enhance the dissimilarity between different rock types in the scene, plots with a higher reflectance were kept in the numerator and plots with low reflectance were kept in the denominator, while taking the band ratios. Using this approach, a ratio of 5/3 was taken for basalt, 7/3 for peridotite, and 4/2 for vegetation.

Figure 3 displays a Band Ratio image (5/3, 7/3, 4/2), in which peridotite appears dark yellowish black colour. It is difficult to distinguish between gabbro and basalt, due to their similar reflectance properties.

In general, the spectral band ratio technique is helpful to identify the peridotite, but basalt and gabbro are not uniformly separable over the entire region.

Principal Component Analysis

Principal Component Analysis (PCA) is a complex statistical approach for highlighting the variance in the image using multiplication of original data with eigenvectors. (NASA Remote Sensing

Tutorial by Dr. Short S.; Lillesand *et al. 2007*). ETM+ data of the study area (band 1 to 5 &7) have been processed in ENVI 4.4 to produce six new PCA bands.

PCA analysis helps to identify the spectral differences of the rock. Every specific rock appears in a divergent colour in RGB composite image of PCA bands (Krishnamurthy 1997). False colour composite image of PCA bands 5, 4, and 2 have been generated as RGB. Geological information of the previously mapped region (Mungall 2007) was compared with the corresponding area within the resultant PCA image (Fig. 4). Uniform correlation between the specific colour and rock type was observed

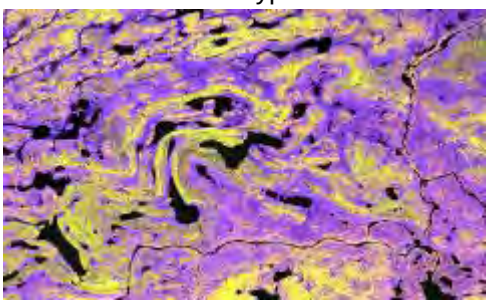

Fig. 3. Band ratio image of 5/3, 7/3, 4/2 as RGB false colour composite.

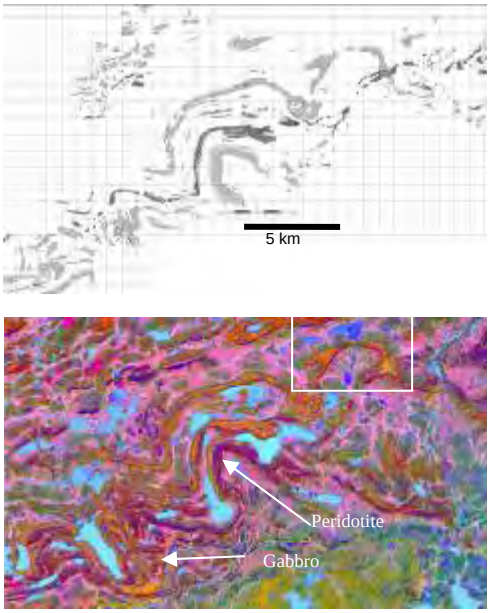

Fig. 4. Comparison of Geological Map and PCA image with Bands 5, 4, 2 as RGB

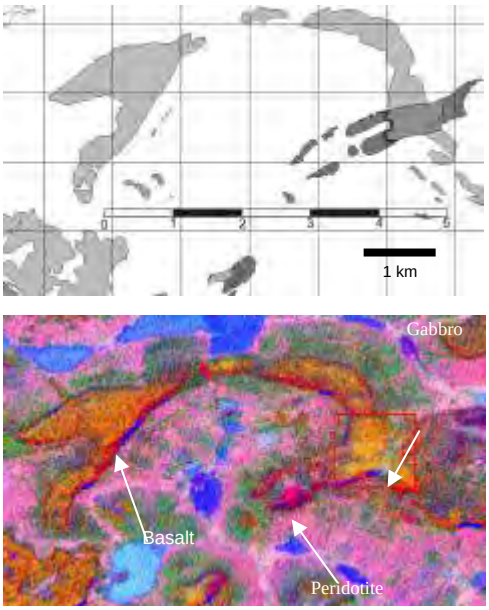

Fig. 5. Comparison of Geological Map and PCA image showing distinction between gabbro, peridotite (Expo Intrusive Suite), meta-basalt (Upper Beauparlant Formation).

throughout the previously mapped area. It validates the possibility of locating the similar rocks in the unmapped neighbouring region with acceptable accuracy.

As displayed in Figure 4, basalt, gabbro, and peridotite has distinctly different spectral signature and shows texture variations between different rock types.

A small subset (within Marked square) of Figure 4 is expanded in Figure 5. Gabbro unit of Expo Intrusive suite (appears light orange) is clearly differentiated from metabasalt (appears orange-black) of the Beauparlant Formation and peridotite (appears dark magenta) of the Expo Intrusive Suite in Figure 5.

Supervised Classification

Supervised Classification was used for accurately categorizing lithology in the study area. PCA bands were used as a basis for identifying the presence of peridotite, gabbro, metabasalt and metasediments and defining the training areas for performing Supervised Classification (Lillesand *et al. 2007*). Area

(pixels) with the preponderance of peridotite, gabbro, metabasalt and metasediments are displayed in red, green, blue and white colours respectively in the output image. The Mahalanobis distance classifier has been run in Envi 4.4 for extracting the similar statistical data pertaining to each class. A small section of the resulting output image is represented in Figure 6, depicting presence of various rocks. At some places, mixing of classes has been observed due to similar appearance of gabbro and basalt in the available ETM+ data.

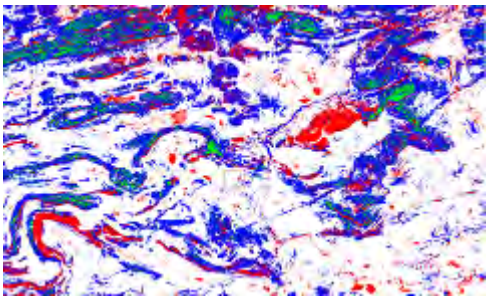

Fig. 6. Supervised Classification image with peridotite, gabbro, metabasalt, metasediments, are shown as Red, Green, Blue, and Yellow.

CONCLUSIONS

Remote sensing techniques have been successfully applied for the identification of rocks in Cape Smith fold belt region. Principal Component Analysis is very effective for the separation of gabbro, metabasalt and peridotite. Band Ratio was helpful for the preliminary identification of peridotite. Supervised Classification approach is taken to verify the results obtained by Principal Component Analysis and Band Ratio. It is also useful to remap the unknown regions once the results are verified.

ACKNOWLEDGEMENTS

I am sincerely thankful to the Canadian Royals Inc for providing Landsat images of the study area. To Dr. Derek Rogge; Research Associate University of Victoria for clarifying my doubts in the fundamental remote sensing principals.

REFERENCES

GAD, S. & KUSKY, T. 2005. Lithological mapping in the Eastern Desert of Egypt, the Barramiya area, using Landsat thematic mapper (TM). *Journal of African Earth Sciences,* ***44,*** 196-202.

KHAN S.D., KHALID MAHMOOD, K, & CASEY, J.F. 2006. Mapping of Muslim Bagh ophiolite complex (Pakistan) using new remote sensing, and field data. *Journal of Asian Earth Sciences,* ***30,*** 333-343.

KRISHNAMURTHY, J. 1997. The evaluation of digitally enhanced Indian Remote Sensing Satellite (IRS) data for lithological and structural mapping. *International Journal of Remote Sensing,* **18**, 3409-3437

MUNGALL J.E. 2007. Crustal Contamination of Picritic Magmas During Transport Through Dikes: the Expo Intrusive Suite, Cape Smith Fold Belt, New Quebec. *Journal of Petrology,* ***48,*** 1021-1039.

SABINS, F.F. 1999, Remote sensing for mineral exploration. *Ore Geology Reviews,* **14,** 57-183.

LILLESAND, T.M., KIEFER, R.W., & CHIPMAN, J. W. 2007. Remote sensing and Image Interpretation, 6th Edition, Chapter seven: *Digital image interpretation and analysis*, pp. 482-623.

Shelat, Y. 2008. Lithological separation using Remote Sensing applications. Undergraduate Research Project Report, University of Toronto, Toronto, ON.

NASA Remote Sensing tutorial by Dr. Short N. http://rst.gsfc.nasa.gov/U

USGS Spectral Library http://speclab.cr.usgs.gov/spectral.lib06/ds231/datatable.html

Selective geochemical extraction patterns in Cyprus soils: responses to geology and land use variations

Nyree Webster[1], David Cohen*[1], Neil Rutherford[12], Andreas Zissimos[3], & Eleni Morisseau[3]

[1]School of BEES, University of New South Wales, Sydney, NSW, 2052, AUSTRALIA
(e-mail: d.cohen@unsw.edu.au)
[2]Rutherford Mineral Resource Consultants, Coogee, NSW, 2034, AUSTRALIA
[3]Geological Survey Department of Cyprus, Strovolos, CYPRUS

ABSTRACT: The regolith of Cyprus has been highly disturbed due to a long history of human occupation and resource exploitation. Selective extraction analysis of surface and subsurface regolith samples from a NE trending transect across Cyprus indicates soil characteristics to be dominated by parent geology material with current land-use having little significant impact on element concentrations.

KEYWORDS: *Soil, selective extractions, Cyprus, atlas*

INTRODUCTION

Cyprus is divided into four east-west trending geological terrains (GSD 2002) ranging from the mafic-ultramafic Troodos Ophiolite Complex and mixed lithologies of the Mamonia terrain to the calcarenite-dominated Circum-Troodos Sedimentary Succession (CTSS) and the volcanic Kyrenia terrain in the north. The Troodos Ophiolite Complex contains a core of ultramafic rocks surrounded by a large sequence of sheeted dolerites, gabbro dykes and overlying pillow basalts which host a number of Cyprus-style Cu sulfide deposits. The geology is the result of a series of multifaceted and inter-related tectonic processes over the period of the Late Cretaceous – Pleistocene.

The Mediterranean region has supported a population dependent upon agriculture for more than eight millennia (Butzer 2005). As a result of a long history of human occupation and resource exploitation the regolith in Cyprus exhibits significant disturbance. Cyprus has been subjected to increasing development over the last thirty years (Robertson & Xenophontos 1997). The lowlands areas are heavily terraced and dominated by agricultural activities, the lower mountain slopes utilised for vineyards, orchards and grazing and the higher elevations are dominated by forests. Soil and regolith profiles from the coast to Troodos vary with skeletal A horizons directly overlying the C horizon in some areas (Cohen & Rutherford 2007).

SAMPLING AND EXPERIMENTAL

Regolith samples were collected from 68 sites along a transect extending from the CTSS in the SW of the island (near Πέτρα του Ρωμιού), across Troodos and into the CTSS and fanglomates on the NE side of Troodos (near Λευκωσία). ICP-MS trace elements concentrations were determined following two conventional (sequential) leaches on the <2mm fraction of the upper (0-25 cm) and lower (50-75 cm) parts of the profile: 1M ammonium acetate in pH 5 acetic acid and 1M hydroxylamine.HCl in pH 1 HCl.

Multivariate analytical methods were applied to investigate any relationships between soil characteristics, geology and land use.

RESULTS

The major geological boundaries correspond with sharp changes in the selective extraction geochemical patterns (Fig. 1). The Troodos ultramafics are characterised by much higher AAC-

extractable Al than other lithologies which may be related to the high proportion of clays derived from the breakdown of plagioclase. AAC Ca is consistently between 12 and 16% in the CTSS unit SW of Troodos (Pakhna Fmn calcarenites) but less than 0.1% in the soils derived from the sheeted dykes. Median extractable Cu is generally higher in the subsoil sample (50-75cm depth) than the surface sample, and higher in the AAC than the subsequent HXL extraction. Extractable Cu is generally highest in the zone extending SW from Troodos across the sheeted dykes and pillow lavas compared with other lithologies (Fig. 2).

Multivariate analysis emphasises the geochemical differences between geological terrains in Cyprus (e.g., Troodos versus CTSS). Factor analysis of the (post-AAC) HXL extraction for the sub-soil samples (Fig. 3) indicates strong separation between samples grouped by parent geology, but a lack of clustering evident when viewed from the perspective of landuse except the clustering associated with forests as these areas are largely restricted to the mafic and ultramafic rocks of the central Troodos region.

CONCLUSION

Geology appears to be the main determinant of trace-element contents and mineralogical form – as defined using selective extractions. There is no indication that landuse *per se* has had a significant general effect on soil trace element geochemistry.

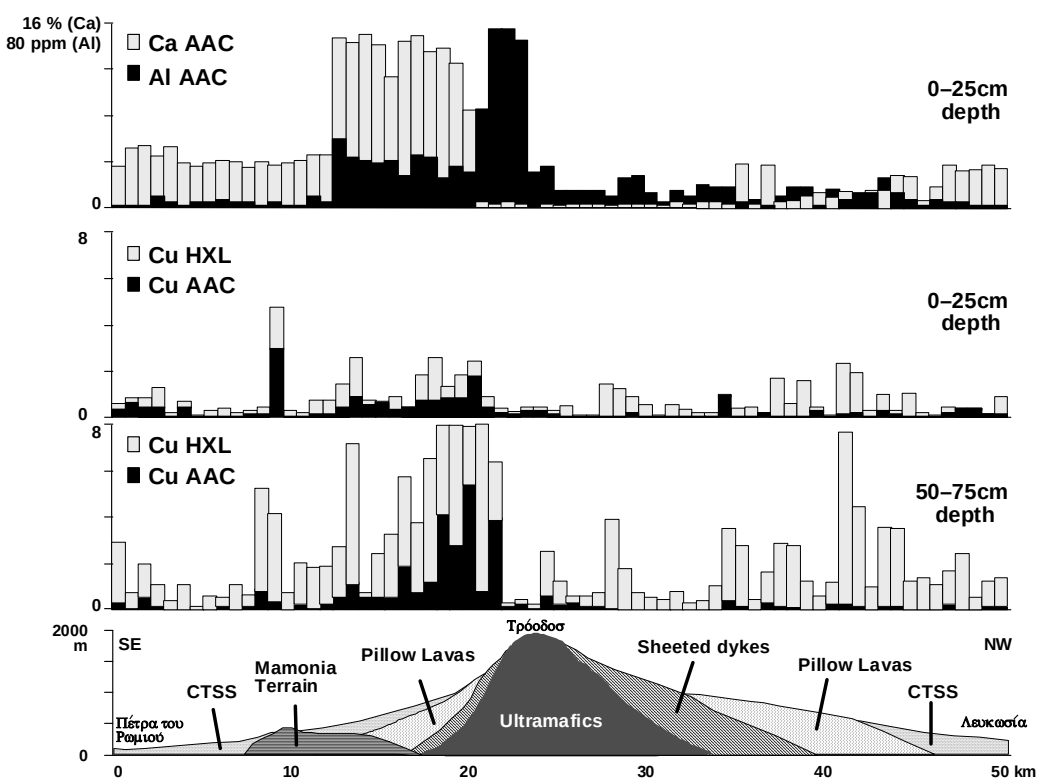

Fig 1. Variation in AAC-extractable Ca, Al and Cu, and HXL-extractable Cu in soils from a NW-trending traverse across Cyprus.

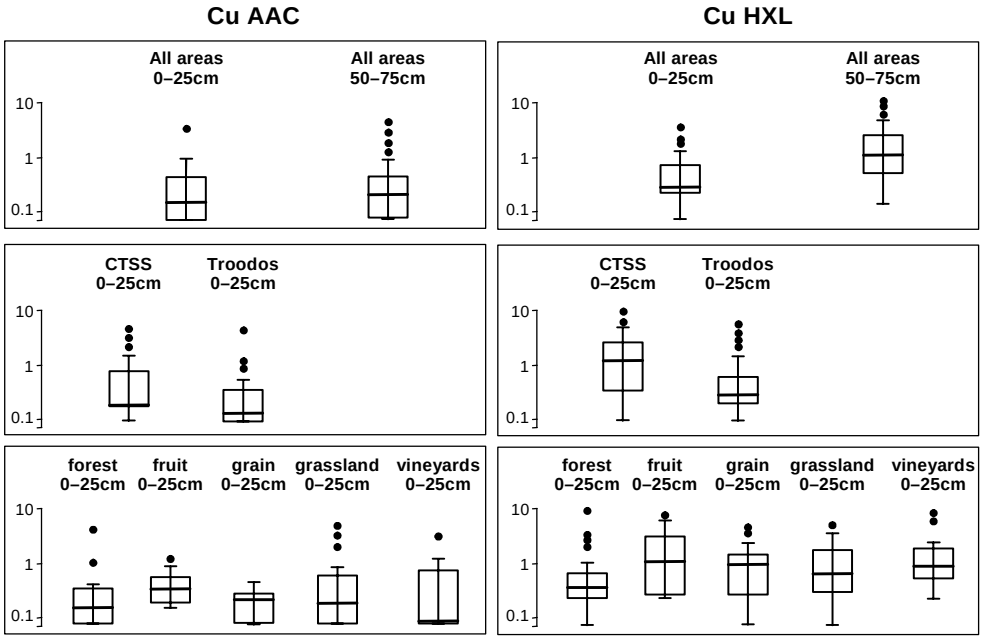

Fig 2. Boxplot comparison of various groupings of AAC and HXL Cu values.

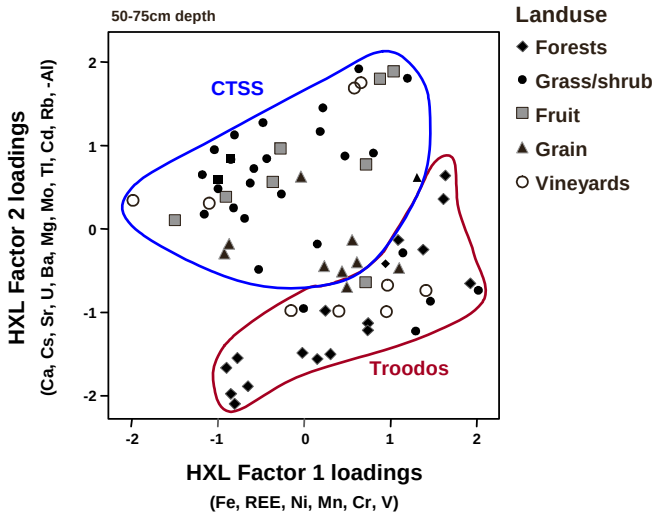

Fig 3. Factor 1 and 2 scores for (post-AAC) HXL-extraction data from the sub-soil samples.

REFERENCES

BUTZER, K.W. 2005. Environmental history in the Mediterranean world: Cross-disciplinary investigation of cause-and-effect for degradation and soil erosion. *Journal of Archaeological Science*, **32**, 1773-1800.

COHEN, D.R. & RUTHERFORD, N. 2007. *Geochemical Atlas of Cyprus, Progress Reports*. UNSW Global.

GEOLOGICAL SURVEY DEPARTMENT OF CYPRUS 2002. *The Geology of Cyprus*. G. Petrides (ed). GSD Publication no. 10,.

ROBERTSON, A.H.F & XENOPHONTOS, C. 1997. Cyprus. In: M.M. Eldridge and W.F. Rhodes (eds), *Encyclopedia of European and Asian Regional Geology*. Chapman & Hall.

The petrogenesis of the Ulsan carbonate rocks from the southeastern Kyongsang Basin, South Korea

Kyounghee Yang
Division of Earth Environmental System, College of Science,Pusan National University, Pusan, 609-735 SOUTH KOREA (e-mail: yangkyhe@pusan.ac.kr)

ABSTRACT: The petrogenesis of the Ulsan carbonate rocks in the Mesozoic Kyongsang Basin of South Korea, which have been previously interpreted as limestone of Paleozoic age, is reconsidered. A small volume of carbonate rocks containing a magnetite deposit and spatially-associated ultramafic rocks is surrounded by sedimentary, volcanic and granitic rocks of the Mesozoic age. The simple crosscutting relationships and other outcrop features indicate that the carbonate rocks are an intrusive phase and younger than the other surrounding Mesozoic rocks. The Ulsan carbonates have low concentrations of REEs and trace elements with the carbon and oxygen isotope values in the range of $\delta^{13}C_{PDB}$=2.4 to 4.0‰ and $\delta^{18}O_{SMOW}$=17.0 to 19.5‰. The outcrop evidence and geochemical signatures indicate that the Ulsan carbonates were formed from crustally-derived carbonate melts, which were generated by the melting/fluxing of crustal carbonate materials owing to the emplacement-related processes of alkaline A-type granitic rocks. Compared to typical mantle-derived carbonatites associated with silica-undersaturated, strongly peralkaline systems, the relatively small size and geochemical characteristics of the Ulsan carbonates may reflect carbonatite genesis in a silica-saturated, weakly alkali intrusive system.

KEYWORDS: *Ulsan carbonate rocks, Kyongsang Basin, magnetite deposit, melting/fluxing of crustal carbonate melt, Alkaline A-type granitic rocks*

INTRODUCTION

The Ulsan carbonates (Fig. 1) have long been interpreted as limestone of Paleozoic age or "age unknown" and as the host of a skarn-type iron (magnetite) deposit due to the intrusion of Cretaceous granitic rocks (Park & Park 1980; Choi *et al*. 1999). However, a Paleozoic marine limestone hypothesis fails to explain the spatial association or the relationship between carbonate and ultramafic rocks in a concentric, ellipsoidal shape surrounded by Cretaceous sedimentary, volcanic, and granitic rocks. The sedimentary hypothesis also fails to explain the isolated exposure of a funnel-shaped Paleozoic marine limestone where no marine limestone has been previously observed within the Mesozoic Kyongsang Basin.

Carbonatites have been defined as rare-metal-bearing rocks composed mainly of carbonate of mantle origin, formed in close association with alkaline rocks (Woolley & Kempe 1989). However, there remains a debate regarding crustal- and mantle-derived carbonate magma or between magmatic differentiation and primary mantle melt. Lentz (1999) postulated a genetic relationship and a possible geochemical continuum between magmatic-hydrothermal skarn systems and some carbonatite systems suggesting a limestone melting/fluxing hypothesis.

Re-evaluating the origin of the Ulsan carbonates can be very important in understanding the geology and petrogenesis in the Mesozoic Kyongsang Basin, South Korea. This present work is summarized and reviewed from the Yang *et al.* (2003).

GEOLOGICAL SETTING

The geology of the study area consists of Cretaceous sedimentary, volcanic, granitic, ultramafic (serpentinite), and carbonate rocks containing a magnetite-rich pipe and basic dykes (Fig. 1). The sedimentary rocks are intruded by felsic volcanic, granitic and ultramafic rocks,

whereas volcanic rocks occur between granitic and sedimentary rocks. Granites are, classified as I-type, intruded by ultramafic rocks showing sharp contacts. Albitite composed of albite and nepheline observed at the contact between granitic rock and the ultramafic rocks (Choi 1983). In addition, one exceptional A-type alkali granite is exposed 4-5 km northwest from the carbonate rocks; it defined as a hypersolvus alkali feldspar granite containing F-enriched sodic amphibole, riebeckite-arfvedsonite, fluorite, and ferri-annite (Koh *et al*. 1996). The ultramafic rocks consist of partly serpentinized dunite and harzburgite containing amphiboles, chromite, magnetite, and chlorite with numerous crosscutting small faults and calcite and dolomite veins.

The Ulsan carbonates hosting the magnetite pipe are surrounded by the ultramafic and volcanic rocks (Fig. 1). Various sized xenoliths of hornfels fragments (volcanic rocks) and ultramafic rocks are often enclosed by the carbonates. The carbonates are massive without any evidence of bedding. They consist of two types of calcites: One is well-crystallized, fine- to medium-grained calcite, whereas the other is large, pure, white calcite crystals (up to 4-5 cm in diameter), which is associated with basic dykes, massive main magnetite ores and metasomatic minerals, implying that they have recrystallized due to the intrusion of dykes. The very contact between carbonate rocks and sedimentary, granite, and serpentinite could not be observed at the surface, but was found in core samples described below. Metasomatic minerals are found along the contacts between the carbonates and volcanic rocks, as well as sedimentary rocks. They include garnet, clinopyroxene, amphiboles, apatite, chlorite, and epidote. The ore pipe is nearly vertical and extends more than 300 m below the surface. The ore minerals are mainly magnetite with small amounts of scheelite and arsenopyrite. Most of the magnetite ore is associated with pyroxene and garnets. Annual production was 100,000 tonnes of magnetite concentrates (60% of Fe) and

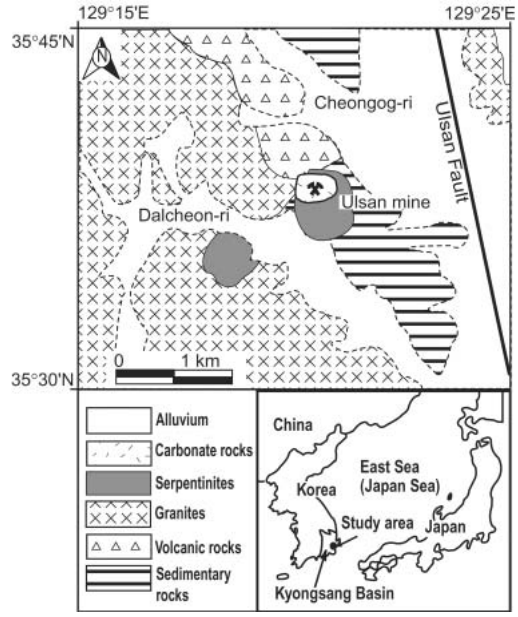

Fig. 1. Geologic map of the Ulsan mining area, South Korea (after Park & Park 1980).

1,200 tonnes of scheelite (74% of WO_3) in 1984.

UNDERGROUND GEOLOGY FROM DRILL CORES

Data from seventy-six exploration drilling core samples collected by Korea Mining Promotion Corporation during 1972-1990 were analyzed in order to understand underground geology in the Ulsan mining area, especially focusing on the relation between the carbonates and the surrounding rocks. The depths of the drill holes reached up to 650 m. Based on the analyses of drill core data, field observations, and previous studies (Park & Park 1980; Choi 1983), a schematic cross-sectional view is constructed. This section clearly shows the ore pipe and carbonate rocks in a funnel-shape surrounded by serpentinite. Most of the magnetite mineralization is observed within the carbonate rocks with only small or trace amounts of magnetite within the serpentinites and hornfels. The carbonates and magnetite pipe are found at the bottom of cores drilled 650 and 300 m deep (Choi 1988), respectively, suggesting they continue farther at depth.

The shape and structure of the carbonates and surrounding rock types suggest the carbonates are an intrusive structure rather than representing a sedimentary sequence.

STABLE ISOTOPES

The carbon and oxygen isotope compositions of the calcites show a bimodal distribution: Group I (fine- to medium-grained calcites) is in the range of $\delta^{13}C_{PDB}$=2.4 to 4.0‰ and $\delta^{18}O_{SMOW}$= 17.0 to 19.5‰, whereas Group II (coarse-grained calcites) is $\delta^{13}C_{PDB}$= -10.3 to -11.1‰ and $\delta^{18}O_{SMOW}$= 9.8 to 11.2‰. Group II values are thought to be modified from Group I. This interpretation is based on their large crystal size and spatial association with dykes. The large calcite crystals possibly resulted from the local recrystallization of fine- to moderately coarse-grained calcite owing to the intrusion of basic dykes. The possible depletion of $\delta^{13}C$ and $\delta^{18}O$ in Group II can be produced by decarbonation or (and) contribution of ^{13}C-depleted carbon from graphite or organic matter in sedimentary wall rocks. Alternatively, the incorporation of significant amounts of CH_4 can be caused by the intrusion of basic dykes.

Compared to typical values from marine limestone, the $\delta^{18}O$ values of Group I are slightly lower, while both $\delta^{13}C$ and $\delta^{18}O$ of Group I are far from those usually associated with carbonatite (Bowman 1998).

RARE-EARTH ELEMENTS AND TRACE ELEMENTS

Trace elements and rare-earth elements (REEs) of the same calcite samples used for the stable isotope analysis have significantly lower concentration of REE as well as most trace elements relative to typical carbonatites. The total REE contents of the Ulsan carbonates range from 3 to 17 ppm, which are much lower than any igneous rocks and even lower than those of some sedimentary rocks. REE and trace-element abundances may have changed sufficiently due to alteration, thus, affecting petrogenetic interpretations for the Ulsan carbonate rocks.

The REE data suggest that these carbonate rocks cannot be carbonatites of mantle origin. However, it is noteworthy that the range of compositional variations of typical carbonatite family rocks overlaps with those of sedimentary, metamorphic, and endogenic carbonate rocks (Samoilov 1991). Samoilov (1991) explained that one reason for the significant compositional variations of the carbonatites were due to different types of the associated alkaline rocks under different geologic–tectonic settings.

DISCUSSION AND CONCLUSION

The Kyongsang basin is composed mainly of Cretaceous-early Tertiary rocks. Paleozoic limestone is reported only in the northern part of the Korean Peninsula up to the present time. Thus, it suggests that the Ulsan carbonates may have been uplifted by the intrusion of granite or transported via a strike-slip fault from the nearest outcrop of limestone 120 km to the south. However, the Kyongsang basin has not experienced any severe deformation since the Mesozoic, rather only sedimentation, uplift, and igneous activity. Moreover, many outcrop observations and cross-cutting relations are inconsistent with the previous ideas. A transportation of a funnel-shaped part of Paleozoic limestone without any of the associated rocks found in the region is geotectonically problematic.

Recent studies regarding carbonatite genesis suggest volatile fluxing and limestone/marble syntectic relationships and crustal carbonate melt generated by intrusion-related pneumatolytic skarn processes may result in geochemical or isotopic compositions that vary within a spectrum of sedimentary crustal to mantle-like igneous sources for carbonatites (Lentz 1998). It is worth noting that an increasing trend of carbonatite magmatism with time has been explained in two different ways: One is due to recycling of more and more crustal carbon (as carbonates) into the mantle since Early Proterozoic (Ray *et al*.

2000), while the other is due to the increased availabilities of intrusion-related syntectic processes with time (Lentz 1999); either assumption reveals more incorporation of crustal carbonate materials with time. In addition, the rare occurrence of carbonatites from oceanic settings was interpreted that crustal carbonate may serve as the source for at least some carbonatites (Hoernle *et al*. 2002).

In conclusion, this study suggests that the Ulsan carbonate rocks are an intrusive phase probably formed by crustal carbonate melt that was generated by the emplacement-related processes of an A-type granitic magma. If an entire spectrum of geochemistry and mineralization can be generated in between two end members, crustal and mantle carbonatite, according to a limestone melting/fluxing theory (Lentz 1999), outcrop evidences obtained from the spatial and simple cross-cutting relations can be decisive criteria for establishing the origin of carbonate rocks of the Ulsan mining area. If the limestone melting/fluxing theory (Lentz 1999) is correct, the relative proportion of carbonate melt generated in the study area is less, reflecting minor carbonatite genesis in association with the silica-saturated, weakly alkalic system.

REFERENCES

BOWMAN, J.R. 1998. Stable-isotope systematics of skarn. In LENTZ, D.R. (ed.) *Mineralized intrusion-related skarn systems*, 99-145. Mineralalogical Association of Canada Short Course 26.

CHOI, S. 1983. *Skarn evolution and iron-tungsten mineralization and the associated polymetallic mineralization at the Ulsan mine, Republic of Korea.* Unpublished PhD. Dissertation, Waseda University, 271 p.

CHOI, S., SO, C., YOUM, S. & KIM, M. 1999. Stable isotopeand fluid inclusion studies of iron-tungsten mineralization at Ulsan skarn deposit (Abstract). *Economic and Environmental Geology,* **32**, 148–9.

CHOI, S.Y. 1988. *A study of the origin of serpentinite in Ulsan mine area.* Unpublished PhD. Dissertation, Pusan National University, 87 p (in Korean with English abstract).

HOERNLE, K., TILTON, G., LE BAS, M.J., DUGGEN, S., & GARBE-SCHONBERG D. 2002. Geochemistry of oceanic carbonatites compared with continental carbonatites: mantle recycling of oceanic crustal carbonate. *Contributions to Mineralogy and Petrology,* **142**, 520-542.

KOH, J.S., YUN, S.H. & LEE, S.W. 1996. Petrology and geochemical characterisitcs of A-type granite with particular reference to the Namsan granite, Gyeongju. *Journal of Petrolology of Society of Korea,* **2**, 142-60 (in Korean with English abstract).

LENTZ, D.R. 1998. Late-tectonic U-Th-Mo-REE skarn and carbonatitic vein-dyke systems in the southwestern Grenville Province: a Pegmatite-Related Pneumatolytic Model linked to Marble Melting (limestone syntexis). In: LENTZ D.R. (ed) *Mineralized intrusion-related skarn systems*, 519-657, Mineralogical Association of Canada Short Course **26**.

LENTZ, D.R. 1999. Carbonatite genesis: A reexamination of the role of intrusion-related pneumatolytic skarn processes in limestone melting. *Geology,* **27**, 335-38.

PARK, K.H. & PARK, H.I. 1980. On the genesis of Ulsan Iron-Tungsten deposits. *Journal of Korean Institution of Mining Geology,* **13**, 104-16 (in Korean with English abstract).

RAY, J., RAMESH, R. & PANDE K. 2000. Carbon isotopes in Kerguelen plume-derived carbonatites: evidence for recycled inorganic carbon. *Earth and Planetary Science Letters,* **170**, 205-14.

SAMOILOV, V.S. 1991. The main geochemical features of carbonatites. *Journal of geochemical Exploration,* **40**, 251-262.

WOOLLEY, A.R. & KEMPE, D.R.C. 1989. Carbonatite: Nomenclature, average chemical compositions, and element distribution. In: BELL, K. (ed) *Carbonatites: Genesis and evolution*, Unwin-Hynman, London, 1-14.

YANG, K., HWANG, J. & YUN, S. 2003. The petrogenesis of the Ulsan carbonate rocks from the southeastern Kyongsang Basin, South Korea. *The Island Arc,* **12**, 428-439.

Alteration-Mineralization Pattern and Geochemical Characteristics of Samli (Balikesir) Fe-Oxide-Cu-(Au) Deposit, Turkey

Erkan Yılmazer[1*], Nilgün Gulec[1], & İlkay Kuscu[2]
[1]*Middle East Technical University, Department of Geological Engineering, Ankara TURKEY*
[2] *University of Mugla, Department of Geological Engineering, Muğla TURKEY*
(e-mail: erkanyil@metu.edu.tr)

ABSTRACT: Şamlı Fe-oxide deposit is one of the major iron-oxide producing mines in western Anatolia (Turkey) (with calculated reserve of 96 000 tonnes @ of 50 to 53% Fe, and >1% of copper (locally as high as 6.78% and 7.74% Cu). Gold and Ag range from 5 to 8 ppm, and 23.8 to 66.9 ppm, respectively. The Şamlı deposit is a typical magmatic-hydrothermal system related to emplacement, crystallization and cooling of Tertiary Şamlı pluton. The alteration and mineralization in Şamli Fe-oxide deposit are formed in 3 major successive stages; pre-, syn-, and post-ore stages. Geochemical (+ isotopic) results for altered and fresh rock samples show that the mineralization in the region is accomplished by hydrothermal fluid(s) derived from a magmatic source during the emplacement of the Samli pluton. The Şamlı pluton was derived from a mantle source, which was either previously enriched by small degree partial melts, and/or metasomatized by an ancient subduction. The field characteristics, mineralizing events and alterations, the oxide and sulfide mineralogy, morphology and distribution of the iron-oxide deposits at Şamlı (Balikesir) deposits suggest that it shows characteristics similar to Fe-oxide-Cu-Au deposits.

Keywords: *IRON OXIDE-CU-AU DEPOSITS, NA-CA ALTERATION, ŞAMLI PLUTON, ŞAMLI, BALIKESIR*

INTRODUCTION

The Samlı Fe-oxide deposit (Balıkesir, Western Anatolia-Turkey) is one of the iron-oxide producing mines in western Anatolia. This deposit has long known as a skarn-type Fe-oxide deposit. However, our recent research has revealed that the alteration hosting the iron-oxide mineralization also contains some unusual assemblages, and the sulfide mineralogy with abundant gold content, should not be related to skarn systems.

GEOLOGY

The Şamlı deposit is located within the Sakarya Zone of Turkey, which is made up of arc-trench sequence of Permo-Triassic age, known as Karakaya Formation or Karakaya complex (Okay *et al*. 1990) (Figure 1).This complex was formed during the closing of Paleo-Tethys and unconformably overlying Jurassic-Cretaceous sediments (Akyüz & Okay 1998). The Karakaya Complex consists of a volcanic-volcaniclastic sequence consisting of mafic pyroclastics and tuffs that alternate with carbonates, turbiditic graywackes, and olistoliths of Permian and Carboniferrous ages cut accross by the Şamlı pluton (Leo & Genç 1986; Okay *et al*. 1990).

In the deposit site, Karakaya Complex is characterized by metapelitic rocks, metadiabase, and recrystallized limestone. The metadiabase and recrystallised limestone occur either as blocks within the Karakaya Complex, or as roof-pendants within the Şamlı pluton. The Şamlı pluton is a large, intermediate to mafic intrusive body emplaced into the rocks of Karakaya Complex. The reported K/Ar geochronology on biotite range from 23.5±1.5 Ma to 18.4±2.2 Ma (Watanabe *et al*. 2003; Karacık *et al*. 2008). Aplite, quartz, and rare pegmatite dykes and veins cut both the main granitoid body and the country rocks.

ALTERATION & MINERALIZATION

The alteration and mineralization in the Şamlı deposit is result of a series of 3 overlapping stages (Fig. 2); The pre-ore

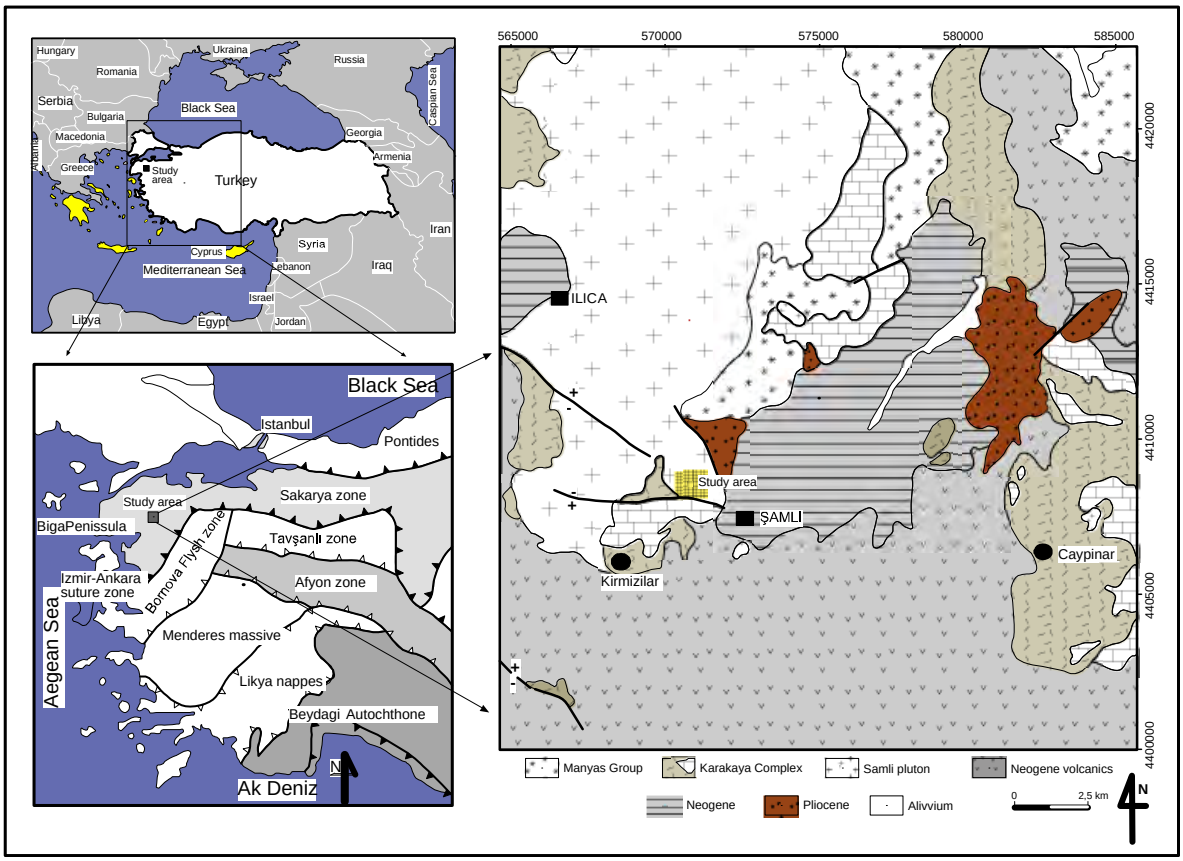

Fig 1. Location & Geological map of Samli-ironoxide deposit.

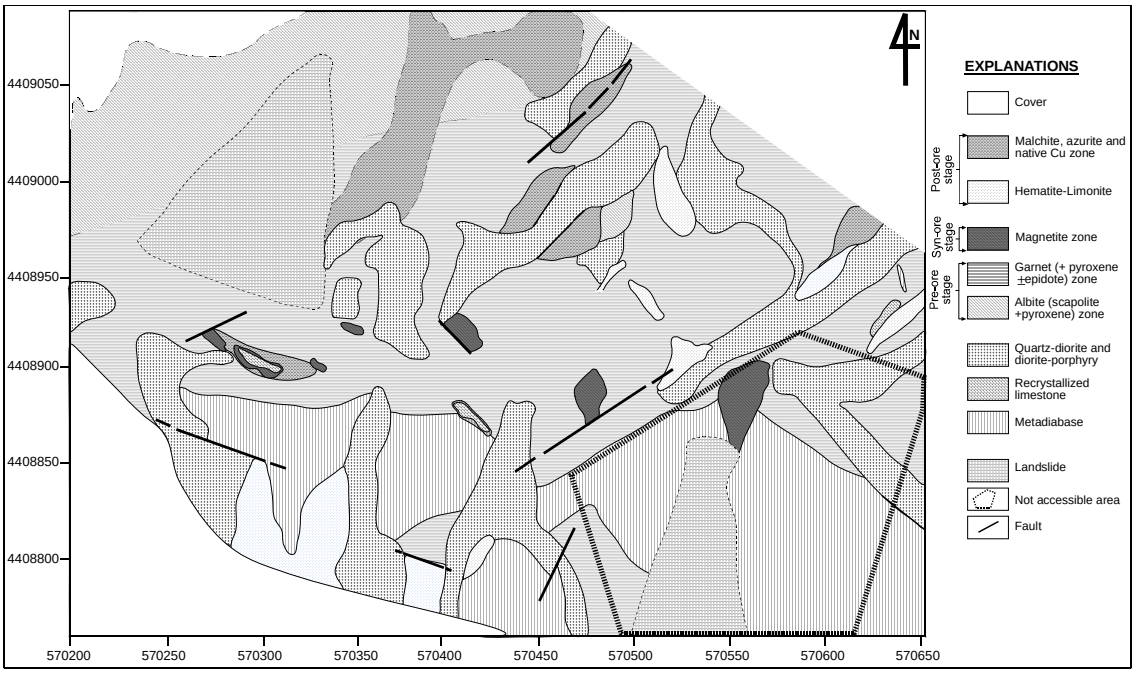

Fig. 2. Alteration-mineralization pattern of Samli Fe-oxide deposit, Turkey.

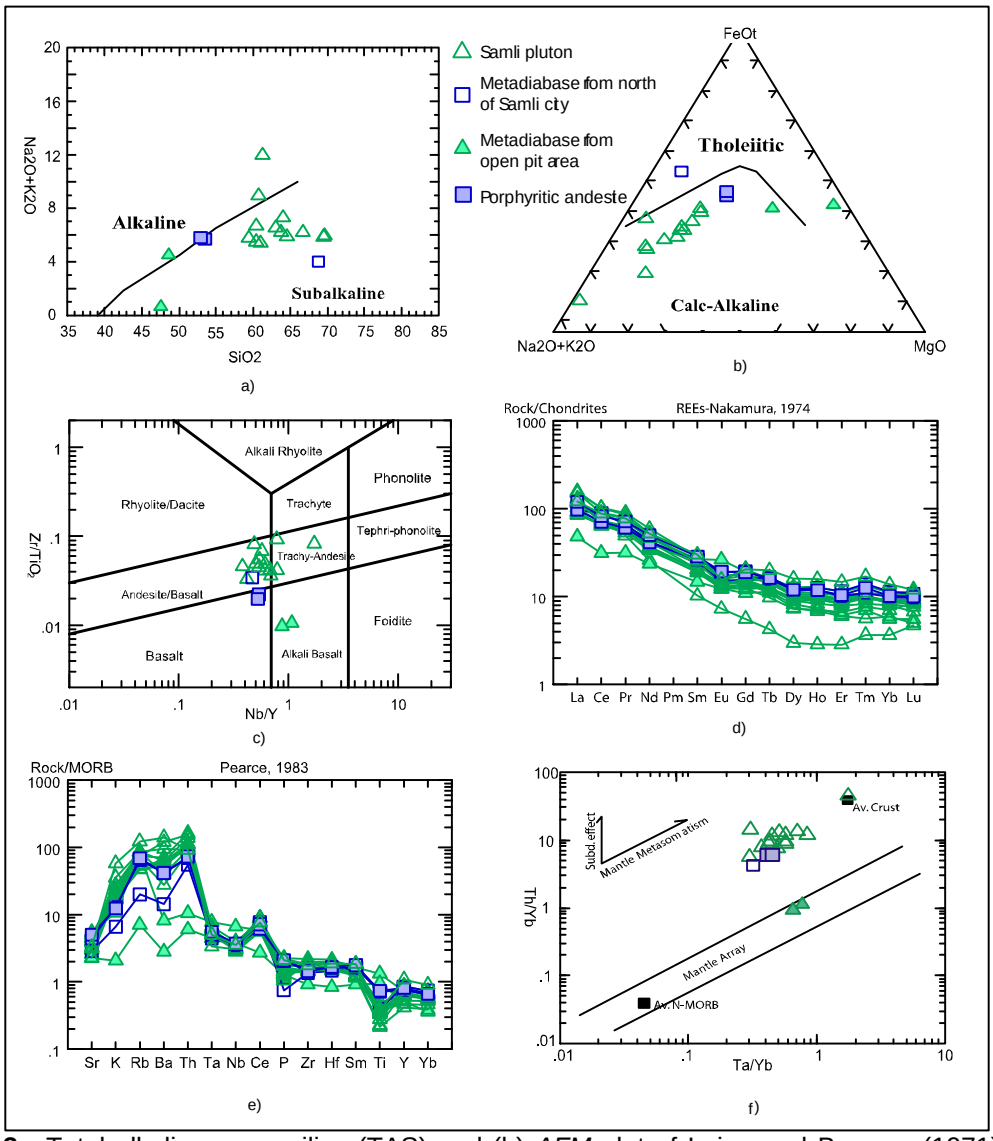

Fig. 3. Total alkalis versus silica (TAS) and (b) *AFM* plot of Irvine and Baragar (1971), (c) modified Zr/TiO2-Nb/Y plot (Pearce, 1996) of Winchester and Floyd (1977), (d) Rock/chondrite-normalized REE diagram for rocks of Şamlı-Ilıca pluton and (e) rock/MORB-normalized spidergrams, (f) Th/Yb vsTa/Yb diagram.

stage refers to Na-Ca alteration including albite (+ scapolite + pyroxene) and garnet-pyroxene (± epidote) alteration assemblage. Syn-ore stage consisting mainly of K-Fe-(Ca) alteration includes magnetite, hydrothermal biotite, epidote, and actinolite. The main magnetite-hematite mineralization is hosted by the syn-ore assemblage. This stage is traced along the pluton-metadiabase/metapelite and pluton- recrystallized limestone contacts and hosted by garnet - pyroxene (± epidote) zone with superimposed albitic alteration. The post-ore stage overprints the Na-Ca and K-Fe assemblages, and consists of chalcopyrite (+epidote +actinolite) hematite-limonite, and Cu-rich (malachite, azurite and native copper) zones. Chalcopyrite, being the most common sulfide, is usually observed as micro-veinlets, together with pyrite in

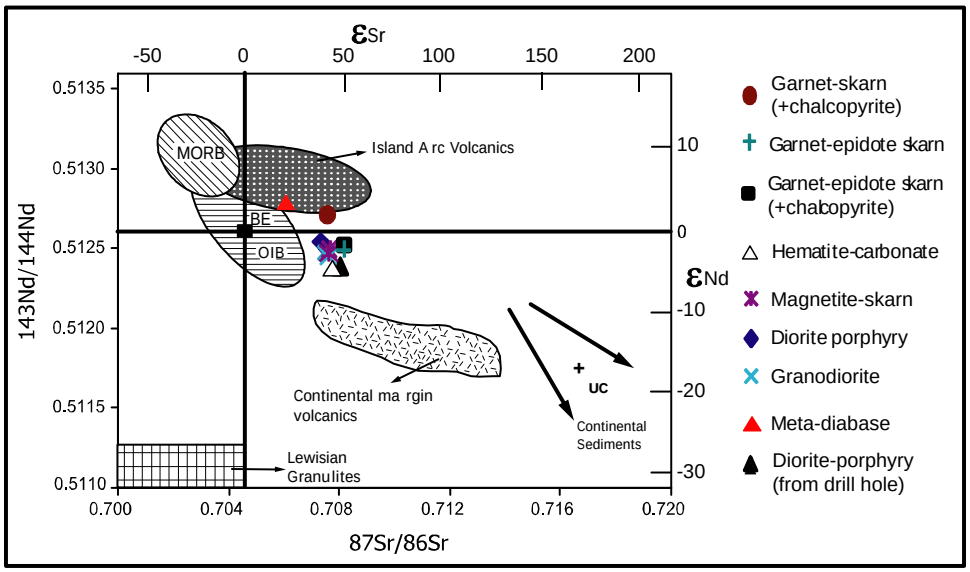

Fig. 4. Nd-Sr isotope correlation diagram.

garnet pyroxene (± epidote) and magnetite zones, while hematite-limonite and Cu-carbonates is only seen as structurally controlled veins and patches in oxidation zones.

GEOCHEMISTRY

The Şamlı pluton is subalkaline and calc-alkaline, and mainly diorite porphyry, granodiorite, quartz monzonite, and granite-porphyry in composition (Fig. 3). The metadiabase is alkali basalt in composition,

based on the major- and trace-element contents. The REE and multielement patterns with significant depletion of Nb and Ta and enrichment of Th and Ba is suggestive of mantle metasomatism or crustal contamination. Likewise, Th/Yb vs Ta/Yb ratios suggests a mantle source, which was either previously enriched by small degree partial melts (displacement along the mantle array), and/or metasomatized by an ancient subduction (Fig. 3).

^{87}SR/^{86}SR, ^{143}ND/^{144}ND, & ^{34}S GEOCHEMISTRY

Results of ^{87}Sr/^{86}Sr and ^{143}Nd/^{144}Nd, and ^{34}S isotope analyses (for both altered and fresh rock samples) range between 0.512361-0.512793 for ^{143}Nd/^{144}Nd, 0.706056 – 0.708167 for ^{87}Sr/^{86}Sr and 0.4-2.6‰ for ^{34}S respectively (Figure 4).

All samples belonging to Samli pluton have a similar ^{87}Sr/^{86}Sr isotope ratio (except for metadiabase characterized by low Sr isotope ratio), suggesting the effect of fractional crystallization process in the genesis of the rocks, although the the possibility of crustal contamination can not be entirely ruled out. Sr-Nd isotope ratios of almost all altered samples show similarity to that of the Şamlı pluton, implying a magmatic source for hydrothermal fluid(s), as is suggested by S-isotope compositions of sulfide samples.

CONCLUSIONS

The Na-Ca and K-Fe-(Ca) alteration assemblage hosting iron-oxide, copper and gold mineralization and spatial and temporal relationship between mineralization and alteration, as well as the oxide and sulfide mineralogy at Şamlı (Balikesir) suggest that it has characteristics more akin to Fe-oxide-Cu-Au systems.

ACKNOWLEDGEMENTS

This work is part of ongoing research project and supported by Middle East Technical University (METU), Project No: BAP-03-09-2007-04. We would like to express our sincere thanks to METU.

REFERENCES

AKYÜZ, H.S. & OKAY, A.İ. 1998. The Geology Of The South of Manyas (Balıkesir) and Tectonic Significance of Blueschists. *Mineral Res. Expl. Bull*., **120**, 81-95.

IRVINE T.N. & BARAGAR, W.R.A. 1971. A guide to the chemical classification of the common volcanic rocks. *Canadian Journal of Earth Sciences*, **8**, 523-548.

LEO, G.W. & GENÇ, M.A. 1986. Geology and iron deposits of the Şamlı area, Balıkesir Province, *MTA*, Türkiye.

OKAY, A.İ., SIYAKO, M., & BÜRKAN, K.A. 1990. Geology of the Biga Peninsula and its tectonic evolution. *TPJD Bull*. (Turkish Association of Petroleum Geologists Bulletin) **2/1**, 83–121 (in Turkish).

KARACIK, Z., YILMAZ, Y., PEARCE, J.A., & ECE, Ö.I. 2008. Petrochemistry of the south Marmara granitoids, northwest Anatolia, Turkey, *International Journal of Earth Sciences*, **97**, 1181-1200.

PEARCE J.A. 1996, A user's guide to basalt discrimination diagrams. In: WYMAN, D.A. (ed) *Trace Element Geochemistry of Volcanic Rocks: Applications for Massive Sulphide Exploration*. Geological Association of Canada, *Short Course Notes*, v.12, p.79-113.

WATANABE, Y., MURAKAMI, H., CENGIZ, İ., SARI, R., KÜÇÜKEFE, S., & VE YILDIRIM, S. 2003. Study on Hydrothermal Deposits and Metallogeny in Western Turkey *MTA*, Ankara.

WINCHESTER, J.A. & FLOYD, P. A. 1977, Geochemical discrimination of different magma series and their differentiation products using immobile elements. *Chemical Geology*, **20**, 325-343.

Total and soil organic carbon, and total sulfur determinations of soils from Cyprus

Andreas Zissimos*[1], Eleni Morisseau[1], Eleni Stavrou[1], & David Cohen[2]
[1]*Geological Survey Department of Cyprus, Strovolos CYPRUS (email: azissimos@gsd.moa.gov.cy)*
[2]*School of BEES, University of New South Wales, Sydney, NSW, 2052 AUSTRALIA*

ABSTRACT: This study is part of the detailed Soil Geochemical Atlas of Cyprus project, involving analysis of 5,520 sites. The general aim of the project is to establish controls on baseline soil geochemical parameters for application in a range of environmental and resource studies. A method has been developed for measuring total carbon (TC), soil organic carbon (SOC) and total sulfur (TS), yielding a limit of quantification of 0.006% TC and 0.003% TS.

KEYWORDS: *Soil, Cyprus, atlas*

INTRODUCTION

Soils are complex materials, containing components of mixed origins with differing physical, chemical and biological properties. The form and concentrations of C and S in soils are important indicators of the environmental status of soils, their agricultural potential and their ability to filter and buffer contaminants (Nuwer & Keil 2005; Rawlins *et al*. 2008; Sylvia *et al*. 2005).

Soils sequester large amounts of C and their capacity to store large amounts of organic carbon (OC) is of considerable importance to modeling the global carbon cycle and, at national scales, allow estimation of soil-related CO_2 emissions as part of commitments to the United Framework Convention on Climate Change (Panagos *et al*. 2008). Modeling requires accurate determination of the portion of inorganically-bound C in soil that is of geogenic origin and tightly bound in various mineral forms (Sahrawat 2003). Carbon is also present in soil biota, micro-organisms and debris of plants, as soil or total organic carbon (SOC or TOC) (Parton *et al*. 1987).

Sulfur enters the current geochemical cycle with the weathering of rocks and conversion to either SO_2 or SO_4^{2-}-bearing species, and subsequent uptake by plants and microorganisms and conversion into a variety of organic forms. Despite the importance of soil C and S in environmental monitoring and modeling, there are no commonly-agreed standards for differentiation of the forms of C and S in soils, and a plethora of measurement methods have been published (Essington 2004; Lorenz *et al*. 2006; Schumacher 2002; Tabatabai & Bremner 1970).

This study forms part of the Geochemical Atlas of Cyprus project, aimed at determining factors broad geological and land-use that control TC, TOC and TS in the soils of Cyprus.

The geology of Cyprus is dominated by four distinct terranes - the Troodos Ophiolite Complex composed of mafic and ultramafic rocks, the Circum-Troodos Sedimentary Sequence containing calcarenites, siltstones and carbonates, the Mamonia Complex composed of igneous, sedimentary and metamorphic rocks and the Kyrenia Terrain containing a series of allochthonous massive and recrystallised limestones dolomites and marbles. These terranes generate highly varied landscapes (Fig 1).

EXPERIMENTAL

The methods for the analyses for TOC and SOC have been developed based on the international standard ISO 10694:1995 and ISO15178:2000.

Soil samples have been collected from

Fig 1. View from edge of Messaoria Plain at Tseri towards dissected palaeo-fan surfaces in middle ground and the Troodos Ophiolite Complex mountains in the background.

the upper 25 cm and the 50 to 70 cm section of regolith profiles at each of 5,520 sites across Cyprus, and sieved to <2mm and milled. A bulk soil sample (CYP-A), derived from a calcarenite is being used as an in-house reference material for testing the analytical protocols.

Samples are oven dried at 100°C after which they are weighed in order to measure water content. TC and TS are measured by introducing dried samples to the Carbon Sulfur (CS) automatic analyzer (Eltra CS-800) instrument. Subsequently, 2g of each sample is introduced in pre-weighed high temperature porcelain crucibles and is introduced to a high temperature muffle furnace for the removal of carbonates at 900°C. Samples are then introduced to the CS automatic analyzer for measurement of organic residual carbon.

For every batch of 20-30 samples a quality control reference material is analysed - either NIST SRM 2711 or CYP-A.

RESULTS AND DISCUSSION

The QC results indicate that the methods developed deliver consistent measurements of TC and TS (Table 1). Measurement of SOC has proven less reliable with a lack of externally certified materials with known values of SOC, or accepted standards to determine SOC. However, a measure of the overall internal precision of our method for measuring SOC indicates reasonably reproducible results (Table 2).

Table 1. Estimates of repeatability (CVr) and reproducibility (CVR) for TC and TS in soil reference materials NIST2710 and 2711.

	TC (%)	TS (%)	TC (%)	TS (%)	TC (%)	TC (%)
CRM	NIST 2711	NIST 2711	NIST 2711	NIST 2711	NIST 2710	NIST 2710
N	76	76	10	10	7	6
Mean	1.739	0.045	1.797	0.041	2.983	0.269
Std Dev	0.044	0.012	0.025	0.002	0.562	0.023
CVR (%)	2.5	26.0			18.8	8.7
CVr (%)			1.4	5.4		

Soil certified reference materials: NIST 2711 *Montana II Soil* %S 0.042 cert. value, %C 2.0 recom. value; NIST 2711 *Montana I Soil* %S 0.240 cert. value, %C 3.0 recom. value

Table 2. Estimates of reproducibility (CVR) for TC, TS and SOC results on in-house soil reference material CYP-A.

	TC (%)	TS (%)	SOC (%)
N	30	29	30
Mean	10.887	0.053	0.171
Std Dev	0.129	0.016	0.047
CVR	1.2	31.0	27.4

Limits of detection (LOD) and limits of quantification (LOQ) for C and S have been evaluated through consecutive measurements of blank crucibles containing accelerator reagents without any sample (Table 3).

The results show good correlation between primary lithological compositions of geological terrains. For example, areas of known sulfide deposits in the Kalavassos area (Fig. 2) show elevated concentrations of TS. Of the ~1000 samples analysed so far in the study, the average TC is 5.304% and average SOC is 1.1%. These values are consistent with data from previous studies on soils in

Cyprus. The average TS value in the soils tested is 0.188%.

The techniques will now be applied to the full sample set collected from 5,520 sites, at an average density of one site per km^2 covering the Republic of Cyprus.

Table 3. LOD and LOQ assessment using blanks.

	TC (%)	TS (%)
N	10	10
Mean	0.0015	0.0009
SD	0.0007	0.0005
LOD	0.002	0.001
LOQ	0.006	0.003

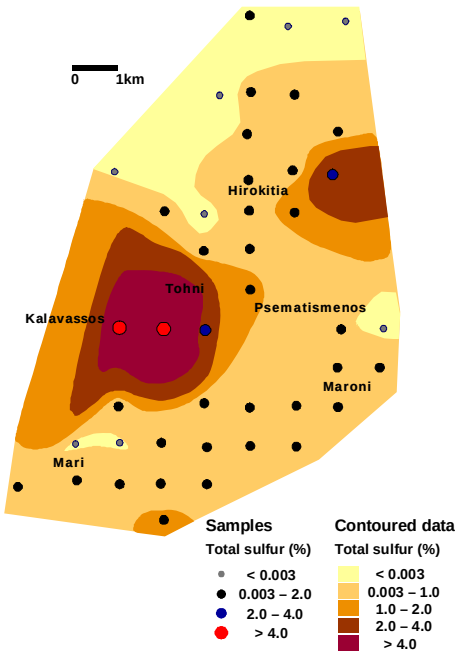

Fig 2. Variation in TS in the top 25cm of soil in the vicinity of the Kalavassos sulfide deposit.

REFERENCES

ESSINGTON, M.E., 2004. *Soil and Water Chemistry: An interactive Approach*, CRC Press.

ISO, 1995. *Soil quality - Determination of organic and total carbon after dry combustion*. ISO standard 10694:1995.

ISO, 2000. *Soil quality – Determination of total sulfur by dry combustion*. ISO standard 15178:2000.

LORENZ, K., PRESTON, C.M., & KANDELER, E. 2006. Soil organic matter in urban soils: Estimation of elemental carbon by thermal oxidation and characterization of organic matter by solid-state ^{13}C NMR spectroscopy. *Geoderma*, **130**, 312–323.

NUWER, J.M. & KEIL, R.G., 2005. Sedimentary organic matter geochemistry of Clayoquot Sound, Vancouver Island, British Columbia. *Limnology and Oceanography,* **50**, 1119–1128.

PANAGOS P., VAN LIEDEKERKE, M., MONTANARELLA, L., & JONES, R.J.A. 2008. Soil organic carbon content indicators and web mapping applications. *Environmental Modelling & Software*, **23**, 1207-1209.

PARTON, W.J., SCHIMEL, D.S., COLE, C.V., & OJIMA, D. 1987. Analysis of factors controlling soil organic matter levels in the Great Plains grasslands. *Soil Science Society of America Journal*, **51**, 1173–1179,

RAWLINS, B. G., VANE, C.H., KIM, A.W., TYE, A.M., KEMP, S.J., & BELLAMY, P.H., 2008. Methods for estimating types of soil organic carbon and their application to surveys of UK urban areas. *Soil Use and Management*, **24**, 47–59.

SAHRAWAT K. L. 2003. Importance of inorganic carbon in sequestering carbon in soils of the dry regions, *CURRENT SCIENCE*, **84**, (7), 10 April.

SCHUMACHER, B.A. 2002. Methods for the determination of total organic carbon in soils and sediments. US EPA Report, NCEA-C-1282, EMASC-001.

SYLVIA, D.M., FUHRMANN, J.J., HARTEL, D.P.G., & ZUBERER, A., 2005. *Principles and Applications of Soil Microbiology*, Pearson Prentice Hall.

TABATABAI M.A. & BREMNER, J.M., 1970. Comparison of Some Methods for Determination of Total Sulfur in Soils. *Soil Science Society of America Journal*, **34**, 417-420.

Sponsors

Symposium bags sponsor

ACME Analytical Laboratories Ltd.

Platinum sponsors

SGS

Anglo American

Gold sponsors

Areva

Newmont

The Gold Company

Barrick

TGI3 Canada

Canada

Silver Standard

maxwell DATASHED

Actlabs

Freewest

Freewest Resources Canada Inc.

Silver sponsors

ODM

Exploring Heavy Minerals

Thermo Scientific

Innov-X Systems

Innovative XRF Technologies

APEGNB AIONB

OZ

xstrata zinc

Adex

Bronze sponsors

PotashCorp

Helping Nature Provide

International Association of Geochemistry IAGC Est.1962

New Nouveau Brunswick

Department of Geology University of New Brunswick

IAG